doi.org/10.26434/chemrxiv.9879947.v1

Water-Soluble Polymeric Carbon Nitride Colloidal Nanoparticles for Highly Selective Quasi-Homogeneous Photocatalysis

Igor Krivtsov, Dariusz Mitoraj, Marina Ilkaeva, Mariana Sardo, Luís Mafra, Christof Neumann, Andrey Turchanin, Chunyu Li, Benjamin Dietzek, Robert Leiter, Johannes Biskupek, Ute Kaiser, Changbin Im, Björn Kirchhoff, Timo Jacob, Radim Beranek

Submitted date: 19/09/2019 • Posted date: 24/09/2019

Citation information: Krivtsov, Igor; Mitoraj, Dariusz; Ilkaeva, Marina; Sardo, Mariana; Mafra, Luís; Neumann, Christof; et al. (2019): Water-Soluble Polymeric Carbon Nitride Colloidal Nanoparticles for Highly Selective Quasi-Homogeneous Photocatalysis. ChemRxiv. Preprint.

Heptazine-based polymeric carbon nitrides (PCN) are well established as promising photocatalysts for light-driven redox transformations. However, the activity of these materials is hampered by their low surface area translating into low concentration of active sites accessible for reactants. Herein, we report, for the first time, a bottom-up preparation of PCN nanoparticles with a narrow size distribution (~10±3 nm), which are fully soluble in water showing no gelation or precipitation over several months, and allow carrying out photocatalysis under quasi-homogeneous conditions. The rate of selective (up to 100%) photooxidation of 4-methoxybenzyl alcohol to 4-methoxybenzaldehyde was enhanced by the factor of 6.5 as compared to conventional solid PCN and was accompanied by simultaneous H_2O_2 production via reduction of oxygen. The dissolved photocatalyst can be easily recovered and re-dissolved by simple modulation of the ionic strength of the medium, without any loss of activity and selectivity. This work thus establishes a new paradigm of easily operable quasi-homogeneous photocatalysis with PCN, and opens up a route for other applications in which liquid aqueous operation or processing of PCN is required.

Water-soluble polymeric carbon nitride colloidal nanoparticles for highly selective *quasi*-homogeneous photocatalysis

Igor Krivtsov*[a,b], Dariusz Mitoraj[b], Marina Ilkaeva[c], Mariana Sardo[c], Luís Mafra[c], Christof Neumann[d,e], Andrey Turchanin[d,e], Chunyu Li[d,f], Benjamin Dietzek[d,e,f] Robert Leiter,[g] Johannes Biskupek[g], Ute Kaiser[g], Changbin Im[b], Björn Kirchhoff[b,h], Timo Jacob[b,I,j], Radim Beranek*[b]

[a] Department of Organic and Inorganic Chemistry, University of Oviedo-CINN, 33006 Oviedo, Spain
Igor Krivtsov

[b] Institute of Electrochemistry Ulm University, Albert-Einstein-Allee 47, 89081 Ulm, Germany
Igor Krivtsov, Dariusz Mitoraj, Changbin Im, Björn Kirchhoff, Timo Jacob, Radim Beranek

[c] CICECO - Aveiro Institute of Materials, Department of Chemistry, University of Aveiro, Campus Universitário de Santiago, 3810-193 Aveiro, Portugal
Marina Ilkaeva, Mariana Sardo, Luís Mafra

[d] Institute of Physical Chemistry and Abbe Center of Photonics, Friedrich Schiller University Jena, Lessingstr. 10, 07743 Jena, Germany
Christof Neumann, Andrey Turchanin, Chunyu Li, Benjamin Dietzek

[e] Center for Energy and Environmental Chemistry Jena (CEEC Jena), Philosophenweg 7a, 07743 Jena, Germany
Christof Neumann, Andrey Turchanin, Benjamin Dietzek

[f] Department Functional Interfaces, Leibniz Institute of Photonic Technology (IPHT), Albert-Einstein-Str. 9, 07745 Jena, Germany
Chunyu Li, Benjamin Dietzek

[g] Electron Microscopy of Materials Science, Central Facility for Electron Microscopy, Ulm University, Albert-Einstein-Allee 11, 89081, Ulm, Germany
Robert Leiter, Johannes Biskupek, Ute Kaiser

[h] Science Institute, University of Iceland, Dunhaga 5, 107, Reykjavík, Iceland
Björn Kirchhoff

[i] Helmholtz-Institute-Ulm (HIU), Helmholtzstr. 11, 89081, Ulm, Germany
Timo Jacob

[j] Karlsruhe Institute of Technology (KIT), P.O. Box 3640, 76021, Karlsruhe, Germany
Timo Jacob

*Corresponding authors: Igor Krivtsov (krivtsovigor@uniovi.es)
Radim Beranek (radim.beranek@uni-ulm.de)

Abstract

Heptazine-based polymeric carbon nitrides (PCN) are well established as promising photocatalysts for light-driven redox transformations. However, the activity of these materials is hampered by their low surface area translating into low concentration of active sites accessible for reactants. Herein, we report, for the first time, a bottom-up preparation of PCN nanoparticles with a narrow size distribution (~10±3 nm), which are fully soluble in water showing no gelation or precipitation over several months, and allow carrying out photocatalysis under *quasi*-homogeneous conditions. The rate of selective (up to 100%) photooxidation of 4-methoxybenzyl alcohol to 4-methoxybenzaldehyde was enhanced by the factor of 6.5 as compared to conventional solid PCN and was accompanied by simultaneous H_2O_2 production *via* reduction of oxygen. The dissolved photocatalyst can be easily recovered and re-dissolved by simple modulation of the ionic strength of the medium, without any loss of activity and selectivity. This work thus establishes a new paradigm of easily operable *quasi*-homogeneous photocatalysis with PCN, and opens up a route for other applications in which liquid aqueous operation or processing of PCN is required.

Introduction

Since the discovery of photocatalytic activity of polymeric carbon nitride (PCN),[1] numerous top-down[2] and bottom-up[3] synthetic strategies aiming to disrupt the strong hydrogen (H-) bonding and van der Waals stacking in bulk-PCN have been reported. These efforts aim at improving the dispersibility of PCN in the reaction medium and to enhance the photocatalytic performance by increasing the number of accessible surface active sites. While top-down methods (*e.g.*, sonication, heat and/or acid treatment) providing low-molecular weight materials proved at least partially effective for achieving this goal, they unavoidably led to reduced yields of the catalyst due to losses occurring during exfoliation[4] or etching[5] and could not achieve truly homogeneous nanoparticles solutions. Another approach is based on breaking of H-bonds in bulk-PCN by dissolving it in appropriate solvents such as concentrated sulfuric acid[6] or sulfonic acid derivatives,[7] which destroys the polymeric structure leading to the formation of discrete PCN species (less than ~1 nm size) and limits the application of the dissolved photocatalyst to aggressive media. Highly alkaline conditions were also applied to obtain water-soluble PCN, however, no photocatalytic activity of the derived gels was reported.[8] Recent efforts regarding bottom-up synthesis of water-soluble or highly-dispersed PCN include templating,[9] high-temperature synthesis in salt melts,[10] electrochemical poly(triazine imide) preparation,[11] sol-gel chemistry using self-induced gelation, occurring within several days, of poly(heptazine imide) hydrosols prepared by the KSCN-assisted condensation of melamine,[12] and formation of water-soluble PCN “quantum dots”, which were highly luminescent, but found to be photocatalytically inactive[13] or their photocatalytic activity was not reported.[2b,3b,14]

Herein, we report, for the first time, a facile and high-yield preparation of PCN nanoparticles with a narrow size distribution (~10±3 nm), which are fully soluble in water showing no gelation or precipitation over several months, and allow carrying out highly efficient photocatalysis *under quasi*-homogeneous conditions. The enhanced performance of this material is demonstrated in *dual-product* photocatalysis involving highly selective (up to 100%) photooxidation of one of the lignin model compounds 4-methoxybenzyl alcohol (4MBA)[15] to 4-methoxybenzaldehyde (4MBAL), concurrent with highly selective (≥70%) reduction of O_2 to H_2O_2, another highly valuable chemical feedstock with a market price higher than, for example, methanol. Finally, we provide a very simple protocol for recovery and re-dissolution of the water-soluble photocatalyst, which

enables easy handling and excellent recyclability of our photocatalyst under *quasi*-homogeneous operation conditions without any apparent loss of activity and selectivity.

Results and Discussion

Synthesis and characterization. Figure 1 shows the schematic representation of the synthesis procedure resulting in a highly active water-soluble and recoverable PCN photocatalyst. Instead of using conventional metal halide-based solvents applied for the preparation of poly(triazine imides) and poly(heptazine imides),[16] or alkali metal hydroxides at high temperature,[17] the use of a KOH/NaOH melt allowed us to reduce the temperature of melamine condensation to PCN structures from the usual range of 500–600 °C, or 450 °C reported by Wang *et al*. for the case of KSCN solvent,[12] down to 330 °C.

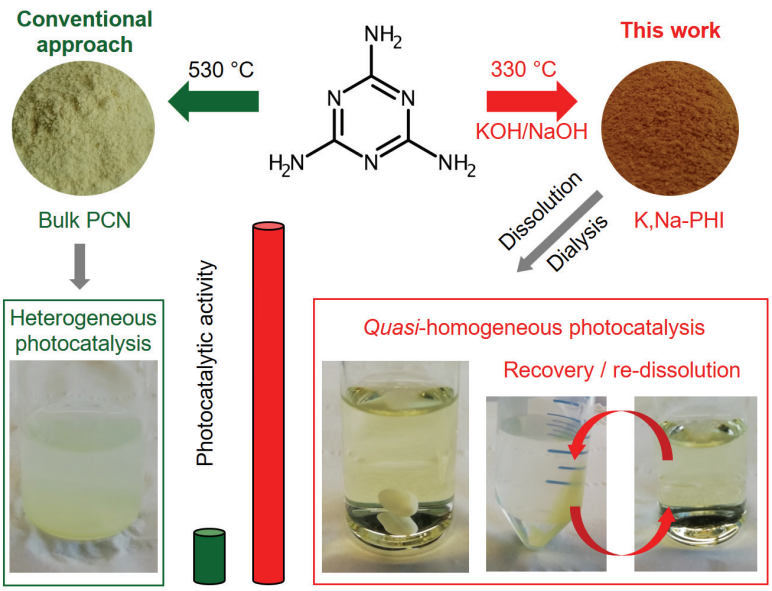

Figure 1. Concept of *quasi*-homogeneous photocatalysis using water-soluble polymeric carbon nitride. Alkali poly(heptazine imide) is synthesized at very low temperature (330 °C) using a KOH/NaOH melt; after dissolution and dialysis the resulting material yields a water-soluble photocatalyst exhibiting photocatalytic rates enhanced by factor of 6.5 as compared to conventional PCN; the water-soluble photocatalyst is easily recovered (by increasing the ionic strength *via* addition of NaCl) and dissolved again, thus enabling excellent recyclability without any loss of activity and selectivity.

The use of KOH at loadings as low as 12.5 mmol (per 1.5 g ~ 12 mmol melamine) in the synthesis yields mostly insoluble potassium poly(heptazine imide) (K-PHI-S) (see Supporting Info, Information, Table S1), while higher loadings (above 15 mmol) result in the formation of a pale-yellow potassium poly(heptazine imide) solution (K-PHI) with very low yield (<9%). The use of

NaOH leads to a water-soluble sodium poly(heptazine imide) (Na-PHI) even at low NaOH quantities (5 mmol), most likely due to its lower melting point, while higher concentrations in the melt induce the degradation of melamine and, consequently, a drastic decrease of the poly(heptazine imide) yield (<4%; Supporting Info, Table S1). The yields of the corresponding dialysed and dried material were highest for melamine condensation in a 10 mmol:5 mmol KOH/NaOH melt (yields up to 42%). The resulting mixed potassium/sodium poly(heptazine imide) (K,Na-PHI) material is water-soluble with a clearly observable Tyndall effect (Supporting Info, Fig. S1). Thermal analysis of the precursor mixture (melamine + KOH/NaOH) shows two main stages of mass loss at 150 and 280 °C assigned to H_2O evolution and to melamine deammonification, respectively (Supporting Info, Fig. S2). The presence of hydroxides in the melt catalyses the condensation of melamine, thus reducing the synthesis temperature of poly(heptazine imide) to 330 °C. This is, to the best of our knowledge, the lowest temperature reported for the solid-state synthesis of heptazine-based PCN materials. The obtained solid (K-PHI-S) and dried solutions of the poly(heptazine imide) after dialysis (K,Na-PHI) show XRD patterns typical for conventional bulk melamine-derived PCN (melon, here designated as CN sample) and low-crystalline poly(heptazine imide) materials with an interlayer spacing of about 3.0 Å and a (100) reflection at 8.9 Å resulting from alkali metal cations incorporated into the poly(heptazine imide) structure[18] (Fig. 2a, Figs. S3 and S4). The structure of the prepared solid K-PHI-S and dried K,Na-PHI samples is also confirmed by FTIR spectra showing a typical fingerprint of PCN materials in the range of 1200 to 1700 cm^{-1}, corresponding mostly to υ(C-NH-C) and υ(C=N) stretching vibrations, and a peak at 800 cm^{-1} attributed to the triazine ring breathing mode.[18] The peak at 3450 cm^{-1}, visible only for K,Na-PHI and K-PHI-S (Fig. 2b), may be assigned to the stretching vibrations of OH-groups incorporated into the poly(heptazine imide) structure as a result of the alkali melt treatment. Additionally, in the range 2150–2175 cm^{-1}, υ(C≡N) vibrations are clearly present in the spectra of the samples prepared in hydroxide melts (Fig. 2b). The same peak assignments can be made regarding the FTIR spectra of K-PHI and Na-PHI (Supporting Info, Fig. S5).

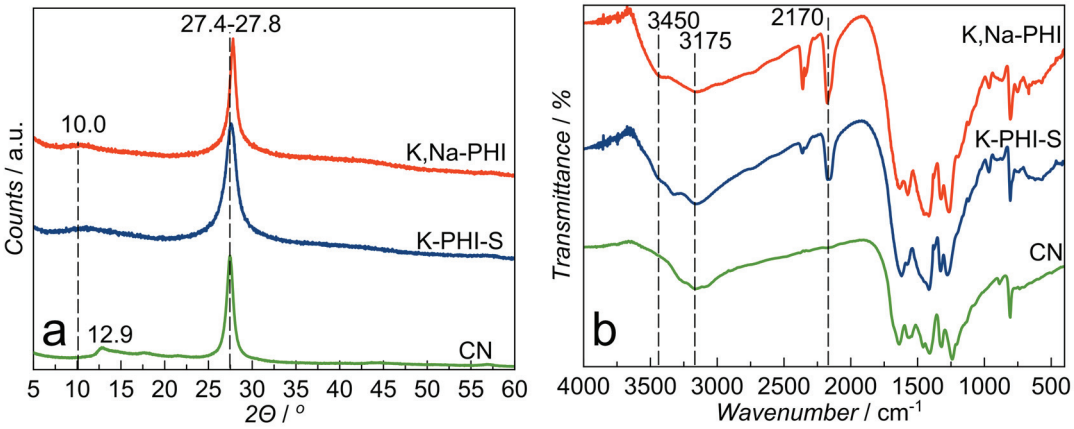

Figure 2. Structural characterization. XRD patterns (a) and FTIR spectra (b) of the prepared materials measured after dialysis and drying.

From all the synthesised series the samples K-PHI-S and K,Na-PHI were chosen for the detailed investigation as being the representatives of insoluble and soluble poly(heptazine imides) (Supporting Info, Table S1). These materials possess a high thermal stability typical for other PCNs, starting to decompose only at temperatures of about 600 °C (Supporting Info, Fig. S6). CHN elemental analysis of the K,Na-PHI and K-PHI-S samples shows a C:N ratios of 0.67 and 0.72, respectively, which are typical for poly(heptazine imide) materials. The reduced concentration of H and the increased C:N ratio observed for K,Na-PHI might indicate a partial loss of NH_2-containing species due to polymer hydroxylation and/or lower fragmentation of the polyheptazine network (Supporting Info, Table S2). The EDX elemental analysis reveals that the content of alkali metals and oxygen is doubled in K,Na-PHI with respect to K-PHI-S (Supporting Info, Table S2). This might be attributed not only to the higher number of surface oxygen-containing functional groups, but also to increased amounts of chemisorbed water and CO_2, whose presence might be responsible for the formation of alkali metal hydroxides or carbonates melting at high temperature (Supporting Info, Fig. S6).

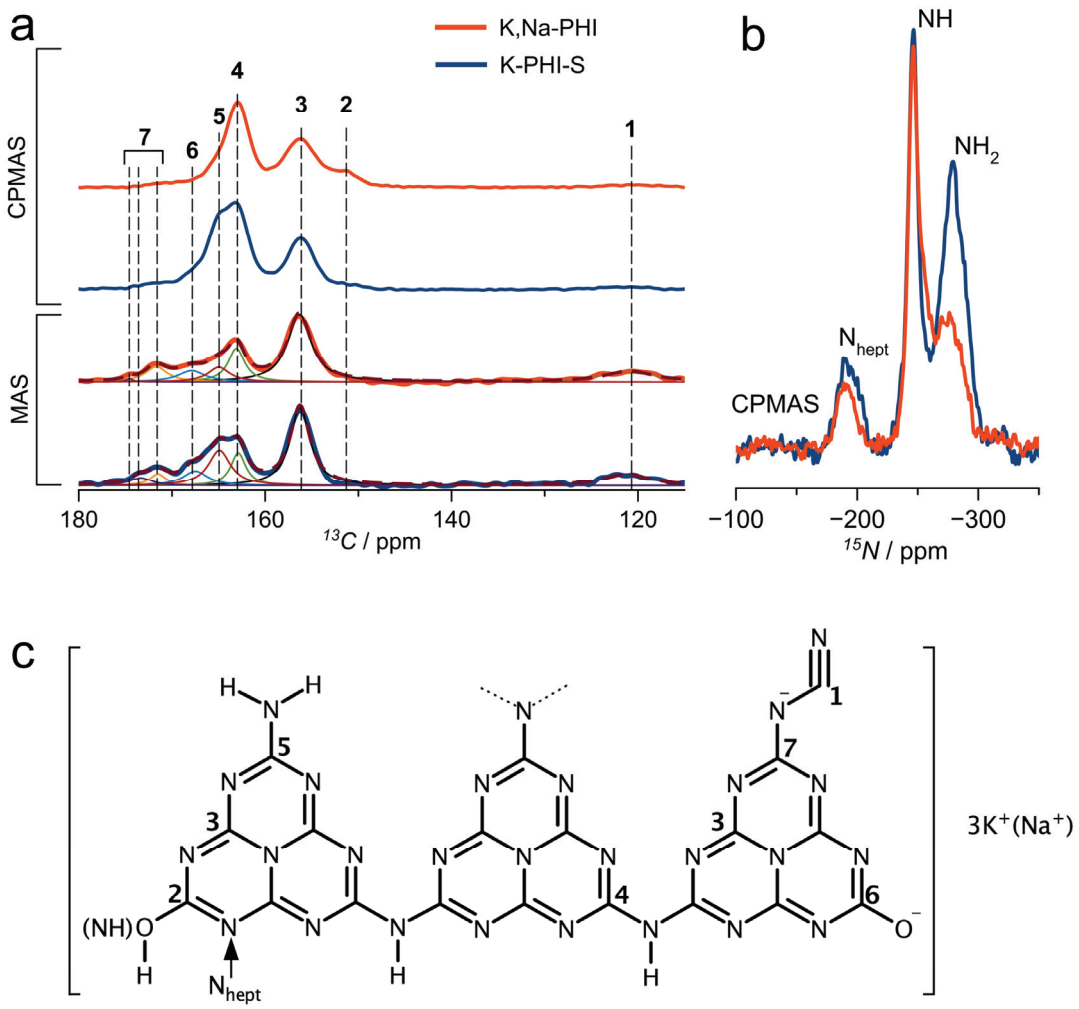

Figure 3. Solid-state NMR analysis: (a) ^{13}C direct excitation MAS and ^{1}H-^{13}C CPMAS (b) ^{1}H-^{15}N CPMAS NMR spectra of K-PHI-S and K,Na-PHI and (c) schematic representation of the functionalized PCN containing numeric labels for resonance assignments. ^{13}C MAS spectra (a) have been deconvoluted showing the different components assigned to the carbon atoms depicted in (c).

In order to obtain further insight into the chemical structure of the materials, solid-state NMR analysis was carried out. ^{13}C direct excitation of the K,Na-PHI sample shows a series of resonances at *ca.* 122, 156, 163, 165, 168 and 169–174 ppm, which are assigned to the carbon atoms in C≡N (**1**), N-C=N (**3**), C-N_2(NH) (**4**), C-N_2(NH_2) (**5**), C-O^- (**6**) and C-N^- groups (**7**), likely found in different environments (Figs. 3a,c and Supporting Info, Fig. S7).[16,19] The presence of CO_3^{2-} species cannot be excluded as its chemical shift coincides with resonances **6** and **7**. The presence of non-protonated N-C=N (**3**) groups suggests the poly(heptazine) nature of the material, although a possible admixture of poly(triazine) units cannot be ruled out completely. In

^{1}H-^{13}C cross-polarization (CP) magic-angle spinning (MAS) NMR spectra of K-PHI-S and K,Na-PHI the resonances ascribed to carbons **4** and **5** are significantly increased with respect to the other resonances (*cf.* CPMAS and MAS, Fig. 3a), while this is not the case for resonances **1**, **3**, **6,** and **7**. A new resonance emerges at *ca.* 151 ppm (**2**) in the ^{1}H-^{13}C CPMAS spectrum of the K,Na-PHI sample, while it is less pronounced for the K-PHI-S sample (Figs. 3a,c, and Supporting Info, Fig. S7). This resonance is tentatively attributed either to the C-OH group of the aromatic poly(heptazine imide) structure or to the deprotonated analogous, *i.e.*, C-O^{-} moieties H-bonded to NH_x resulting from drying and polymerization. A similar observation was made for crystalline potassium cyamelurates and cyameluric acid.[20] A distinguishable shoulder, at *ca.* 165 ppm (**5**), is observed at the left side of the ^{13}C resonance **4** (*ca.* 163 ppm) for K-PHI-S (Fig. 3a), which corresponds to N_2C-(NH_2) and N_2C-(NH) species, respectively. Notably, the resonance at *ca.* 165 ppm (**5**), observed in K-PHI-S, is drastically reduced for K,Na-PHI (Figs. 3a,c, and S7). Resonance **6** at about 168 ppm, observed from the ^{13}C MAS spectrum of K,Na-PHI is not enhanced on the ^{1}H-^{13}C CPMAS spectrum, suggesting the lack of protons in the vicinity of this functional group. This supports the assignment of **6** to C-O^{-} stabilized by K^{+} or Na^{+} such as in the $[C_6N_7O_3]^{3-}$ groups of $K_3[C_6N_7O_3]\times H_2O$.[21] The ^{1}H-^{15}N CPMAS spectra of K,Na-PHI and K-PHI-S show three resonances at *ca.* –275, –246 and –191 ppm assigned to NH_2, NH and heptazine secondary amines (N_{hept}), respectively. Although CPMAS is not quantitative, the NH_2/NH intensity ratio of the K,Na-PHI sample is much smaller than that of K-PHI-S; we hypothesize that NH_2 groups are consumed due to reaction with KOH/NaOH (Fig. 3b,c). Also, a shoulder at –257 ppm, attributed to -N=C-OH(NH) can be observed in the spectrum of the K,Na-PHI sample (Supporting Info, Fig. S7). A quantitative estimation based on the ^{13}C direct excitation MAS spectra (Supporting Info, NMR study, Table S3 and Supporting Info, Fig. S7) suggests that the formation of heptazine species (Supporting Info, Fig. S8) is favoured for the case of the K,Na-PHI sample, resulting in an increased number of N-C=N (**3**) carbons in K,Na-PHI as compared to K-PHI-S (Supporting Info, Table S3, Fig. S7). The lower concentration of terminal -NH_2 moieties in K,Na-PHI will likely lead to an overall decrease of the number of hydrogen bonds in the polymer network, thus exerting a direct influence on aggregation and solubility.

The X-ray photoelectron spectroscopy (XPS) data corroborate the presence of C-O$^-$ species in both analysed samples (Supporting Info, Fig. S9, Table S4) and indicate the redistribution of N-containing groups for the material prepared using KOH/NaOH mixture (Supporting Info, Figs. S9e,f, Table S4). Although C1*s* XP spectra confirm the presence of N-C=N bonds, they do not allow unambiguous assignment of the peak at *ca.* 286.2 eV that may be attributed to C-NH$_x$ and C-O$^-$ groups (Supporting Info, Fig. S9, Table S4). The N1*s* spectra reveal a different distribution of the N-containing species in K-PHI-S and K,Na-PHI. Based on integrated peak intensities, the increased contribution of the peak (C-N=C *plus* C≡N (N1)) with respect to those attributed to N-C$_3$ *plus* triazine C-NH$_x$ (N2) and heptazine C-NH$_x$ (N3) suggests a higher relative content of N belonging to the PCN aromatic structure in the K,Na-PHI material. This indicates a higher degree of condensation (Supporting Info, Fig. S9, Table S4). The O1*s* spectrum also exhibits an additional band at 531.0 eV in K,Na-PHI which can be tentatively assigned to CO_2 chemisorbed by the alkali metal ions present in higher quantities than in the K-PHI-S sample or to the hydroxylated carbon nitride species.

Summarizing, we hypothesize that the K-PHI-S material prepared in KOH melt possesses a poly(heptazine imide) structure bearing NH, -NH$_2$ groups, uncondensed triazine, NH$_x$-containing species and oxygenated surface moieties in the form of cyamelurate fragments. The water-soluble K,Na-PHI prepared in KOH/NaOH mixture is also composed of a poly(heptazine imide) network. However, it is suggested to have a higher number of heptazine nitrogen atoms owing to a higher degree of triazine-to-heptazine condensation and a much smaller number of terminal amines resulting in weaker H-bonding between the poly(heptazine) layers. This—in combination with the presence of terminal cyamelurate functional groups in the material facilitating the formation of a solvent structure around the K,Na-PHI particles—rationalizes its high solubility in water. The dissolved K,Na-PHI has a zeta potential of –31 mV at pH of 7.5; this is a typical value for PCN-derived materials[22] which are prone to agglomeration in suspensions due to strong hydrogen bonding between the terminal NH$_x$ species and the N atoms of the heptazine units. This means that electrostatic repulsion alone cannot be entirely responsible for the excellent dispersion of K,Na-PHI in water. We speculate that in K,Na-PHI, the cyamelurate C-O$^-$ groups are stabilized by hydrogen bonds mainly with water molecules from the well-ordered hydration shell of the Na$^+$ ion. At low concentrations, Na$^+$ ions will therefore promote formation of a hydration

layer at the PHI surface which improves solubility. With increasing Na^+ concentration the hydration layer will gradually be stripped causing coalescence due to positive van der Waals forces (see also Supporting Info, Fig. S10). Notably, we have not found any appreciable solubility of K,Na-PHI in most of the common polar or non-polar *organic* solvents. This corroborates our assumption that the cyamelurate-functionalities of K,Na-PHI specifically interact with water creating a water solvation shell, which hinders the formation of hydrogen bonds with other dissolved species and increases the electrostatic repulsion between nanoparticles due to the negative surface charge.

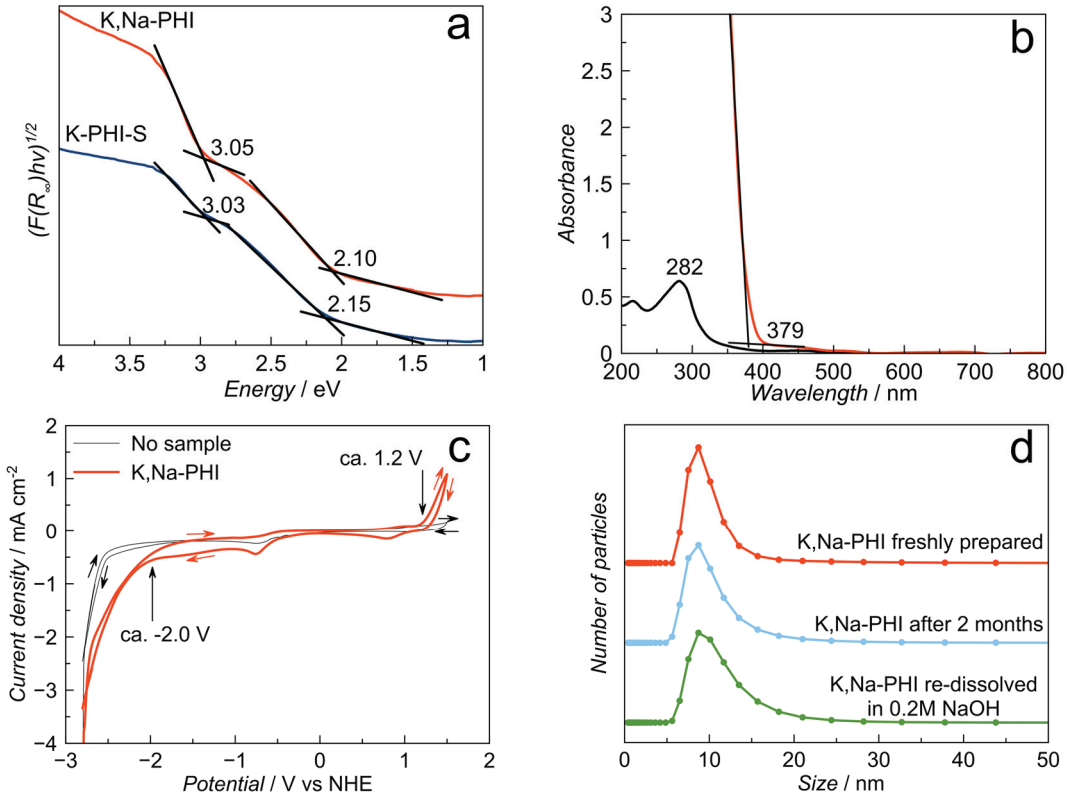

Figure 4. Materials characterization. (a) Diffuse reflectance UV-vis spectra of the solid K-PHI-S and dried K,Na-PHI samples transformed using the Tauc formalism for the determination of absorption edges. (b) UV-vis electronic absorption spectra of K,Na-PHI dissolved in water at concentrations of 0.005 and 0.75 g L^{-1}. (c) Cyclic voltammetry (50 mV s^{-1}, 0.1M $TBAPF_6$ in acetonitrile) of the K,Na-PHI sample deposited on a glassy carbon electrode. (d) Particle size distribution of the PHI samples measured by dynamic light scattering.

Density Functional Theory calculations using an implicit solvation approach on a periodic PHI model are in agreement with this hypothesis (for details, see Supporting Info, Theoretical study of K,Na-PHI). By comparing the stability of the model system (Supporting Info, Fig. S11) in water,

acetonitrile, or methanol environments, we find that water will lead to a higher stabilization than the latter two (see Supporting Info, Table S5). Further, we find that stabilization increases with the number of oxygen-containing moieties.

The analysis of electronic absorption properties of the dried poly(heptazine imide) samples using diffuse reflectance spectroscopy shows the presence of two optical absorption edges at *ca.* 2.1–2.2 and 3.0 eV (Fig. 4a). In contrast, the electronic absorption UV-vis spectra taken from dissolved K,Na-PHI in water do not exhibit any significant light absorption in the visible-range (Fig. 4b). However, it is clear that a maximum absorption edge appears in the UV-range (285 nm) under dilute conditions, while in concentrated solution the absorption edge shifts to 379 nm corresponding to ~3.3 eV (Fig. 4b). The absorption at 285 nm can be attributed to the cyamelurate species present in K,Na-PHI.[20a] The slightly lower-energy absorption edge value of 3.0 eV measured in the solid-state as well as the appearance of the additional absorption edge at 2.1 eV might be attributed to the stacking or coalescence of the poly(heptazine imide) units, contrary to what is observed for the well-separated nanoparticles in a colloidal solution. The cyclic voltammetry study of the K,Na-PHI sample is in agreement with the energy gap determined by the optical method, showing the HOMO and LUMO positions at 1.2 V and –2.0 V *vs.* NHE, respectively (Fig. 4c). The water-soluble K,Na-PHI nanoparticles prepared in this work show a relatively narrow size distribution (~6-20 nm) as determined by dynamic light scattering (DLS; Fig. 4d). The mean particle size of the sample is around 10 nm (Fig. 4d). The alkali poly(heptazine imide) materials prepared using pure alkali metals (Na or K) demonstrate slightly broader size distribution (Supporting Info, Fig. S12). The Na,K-PHI particles are stable in water-based media for several months without suffering agglomeration. Notably, the dried material can also be re-dissolved in 0.2 M NaOH exhibiting a nearly identical particle size distribution, which confirms that the water-soluble PCN nanoparticles retain their morphological and structural integrity (Fig. 4d).

The coalescence of dissolved particles after drying results in almost featureless SEM images, not showing any definite morphology (Supporting Info, Fig. S13). Although we were unable to obtain high-resolution TEM images due to significant beam damage to the samples, fiber-like morphology of the sample prepared from a dilute solution of K,Na-PHI dried on the microscope grid is noted (Supporting Info, Fig. S14). The thickness of the fibers is estimated to be *ca*. 10 nm, which is in agreement with the data from dynamic light scattering (Fig. 4d). Note however, that it

cannot be ruled out that the observed morphology results from coalescence of the particles during the drying procedure. We speculate that fiber net observed in TEM image is a result of the anisotropy of the original PHI particles causing directional agglomeration.

Photocatalytic studies. Pristine and modified PCNs are well-known photocatalysts for partial photooxidation of organic molecules,[23] and methoxy-substituted aromatic alcohols in particular,[24] which opens the route for synthesis of high-value chemicals from low-value feedstock using only sunlight or cost-effective light sources (*e.g.*, LED arrays) and easily available oxidizing agents such as aerial oxygen. The water-soluble colloidal PCN nanoparticles prepared in this work allow, for the first time, to perform photocatalysis with PCN under *quasi*-homogeneous conditions. The optimization of the photocatalyst concentration in the reaction mixture was carried out for the solid K-PHI-S and the water soluble K,Na-PHI samples, resulting in optimal loadings of 0.5 gL^{-1} and 0.75 gL^{-1}, respectively (Supporting Info, Figs. S15, S16). Initial tests for selective photooxidation of 4MBA to 4MBAL in water have demonstrated increased activity of K-PHI-S and K,Na-PHI with respect to the conventional PCN (CN sample) by factors of 2.1 and 2.8 under heterogeneous and *quasi*-homogeneous conditions, respectively (Fig. 5a, Supporting Info, Fig. S17, Table S6). Notably, formation of the aldehyde is accompanied by two-electron reduction of O_2, producing hydrogen peroxide,[25] another highly valuable compound. Using a purely aqueous solvent, the selectivity towards both target molecules after 4 h of irradiation is lower for the most active K,Na-PHI sample as compared to the benchmark CN photocatalyst (Fig. 5a, Supporting Info, Fig. S18, Table S6). Addition of acetonitrile (MeCN), whereby *quasi*-homogeneous reaction conditions are retained below 50 vol% of MeCN (Supporting Info, Figs. S19, S20), was found to significantly increase both activity and selectivity. We hypothesise that addition of MeCN accelerates desorption of the less polar aldehyde from the K,Na-PHI surface (Fig. 5a, Supporting Info, Fig. S17, Table S6). The heterogenization of the reaction medium occurring at concentrations of MeCN > 50 vol% (Supporting Info, Figs. S19, S20) is detrimental for the photocatalytic activity (Fig. 5a, Supporting Info, Fig. S16, Table S6), which confirms the highly beneficial effect of running the reaction under *quasi*-homogeneous conditions. Under optimal reaction conditions (40 vol% of MeCN), the rate of 4MBA oxidation was increased by a factor of 2.3 and 6.5 as compared to the results obtained for K,Na-PHI and for a conventional CN

photocatalyst in H_2O, respectively. Furthermore, selectivities towards the reaction products 4MBAL (91 %) and H_2O_2 (76 %) were enhanced (Fig. 5a, Supporting Info, Fig. S17, Table S6; note that, for the conventional CN, the conversion degree in the presence of MeCN was not enhanced). We point out that at lower conversion degrees (50%) of 4MBA the selectivity is *ca.* 97% and at even lower conversion levels it reaches up to 100% (Supporting Info, Fig. S17, Table S6). It should also be noted that the catalytic performance of the solid heterogeneous photocatalysts, conventional CN and K-PHI-S, is practically not affected by the presence of the organic solvent in the reaction mixture (Supporting Info, Fig. S21). Interestingly, the *quasi*-homogeneous nature of the photocatalytic systems allows to reduce scattering effects on the suspended particles compared to conventional heterogeneous photocatalysis, hence improving the reliability of quantum yield estimations for this system (for details, see the Supporting Info, Information). The K,Na-PHI photocatalysts exhibited a quantum yield of *ca*. 10 % at 365 nm towards the 4MBAL formation, which is a rather respectable value as compared to common heterogeneous photocatalysts that typically show quantum yields of few per cent.[26]

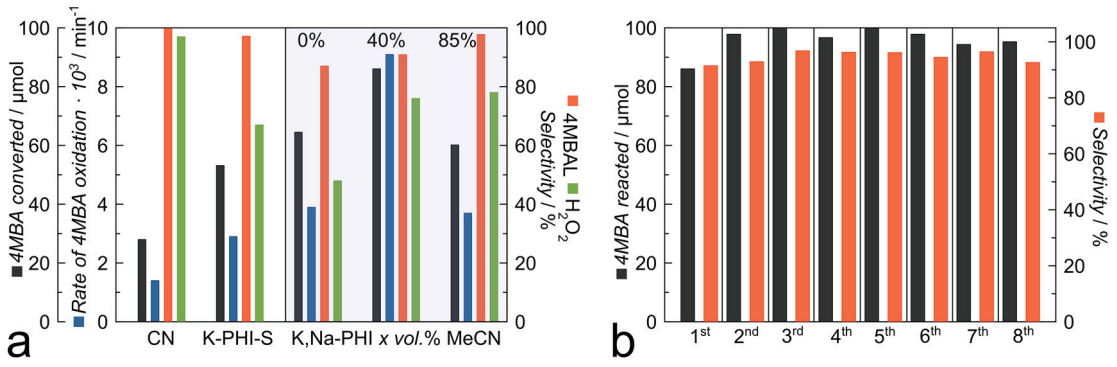

Figure 5. Photocatalytic tests. (a) Photocataytic oxidation of 4MBA with simultaneous H_2O_2 formation in H_2O (20 mL, 4MBA 0.1 mmol, pH 6.5–7.0, LED 365 nm, 4 h) and in H_2O/MeCN mixture in the presence of K,Na-PHI (20 mL, X vol% of MeCN, 4MBA 0.1 mmol, LED 365 nm, 4 h) (b) recyclability test of the K,Na-PHI samples for 4MBA oxidation (20 mL, 40 vol.% of MeCN, 4MBA 0.1 mmol, pH 6.5–7.0, LED 365 nm, 4 h, 0.125 g of NaCl is added for the photocatalyst recovery).

A typical shortcoming of the practical implementation of homogenous or *quasi*-homogeneous photocatalysts concerns difficult recovery for reuse. Interestingly, we find that our water soluble K,Na-PHI photocatalyst can be easily recovered by increasing the ionic strength of the solution which will causing coagulation and precipitation of K,Na-PHI. This can be achieved by addition of a salt such as NaCl (Fig.1, Supporting Info, Fig. S10). The photocatalyst can then be centrifuged,

separated from the liquid phase, and re-dissolved. With this protocol, the photocatalyst can be reused in water as well as in H_2O/MeCN(40 vol%) medium for at least eight reaction cycles without any deterioration of its activity or selectivity (Fig. 5b, Supporting Info, Fig. S22).

In-situ absorption and emission spectroscopy was performed to gain further insight into the photocatalytic performance of the water-soluble K,Na-PHI photocatalyst. Fig. 6a shows stable absorption spectra of K,Na-PHI over a period of 4 h, when dissolved in degassed water. Under ambient atmosphere, a slight change of the absorption band at around 280 nm is apparent during the first hour of irradiation. Subsequently, the photoinduced changes in the colloidal solution level off, reaching a state in which the absorption spectrum changes no further. Similar changes are observed in *in-situ* emission spectroscopy, in which the sample is continuously irradiated by an LED at 365 nm, while the fluorescence is intermittently (every five minutes) excited at 275 nm (Fig. 6b). In the absence of atmospheric oxygen (spectra recorded at 0, 5 and 10 minutes) the emission intensity is stable. Upon exposing the sample to air, the emission intensity drops in the course of the first hour, after which the changes level off. These data point to the colloidal nanoparticles solution being a dynamic system in which a stable stationary state develops over time when the system is irradiated while in contact with air. Fig. 6c shows a fluorescence titration of K,Na-PHI in water upon addition of 4MBA. Upon addition of the substrate, the emission band associated with the alcohol itself (at 300 nm) increases, while the emission of the K,Na-PHI decreases, indicating interaction of the photoexcited photocatalyst with the substrate. The fact that both dioxygen and 4MBA quench effectively the emission of the photoexcited K,Na-PHI corroborates its high activity in simultaneous photooxidation of 4MBA and reduction of O_2 to H_2O_2.

The high photocatalytic activity of the K,Na-PHI photocatalyst along with its solubility in water represent a great promise for its use in light-driven valorization of low-value feedstock such as insoluble lignocellulosic substrates,[27] where conventional solid-state CN materials would be inefficient due to their low surface area hampering the accessibility of substrates to the active sites. In this context, it is noteworthy that catalysts of PCN family are not only capable of oxidation of benzylic C-OH, but also of benzylic -CH_3 oxidation reactions in model lignin compounds.[28] Finally, we note that while the K,Na-PHI is fully water-soluble in a wide pH range (5-13), it can be converted into a gel simply by adding a strong acid, such as HCl. Therefore, we anticipate that the here presented water-soluble carbon nitrides can be utilized not only in any applications

requiring aqueous liquid processing of carbon nitride, but also as building blocks in fabrication of further novel photocatalytic architectures with tailored morphology and porosity using sol-gel chemistry.

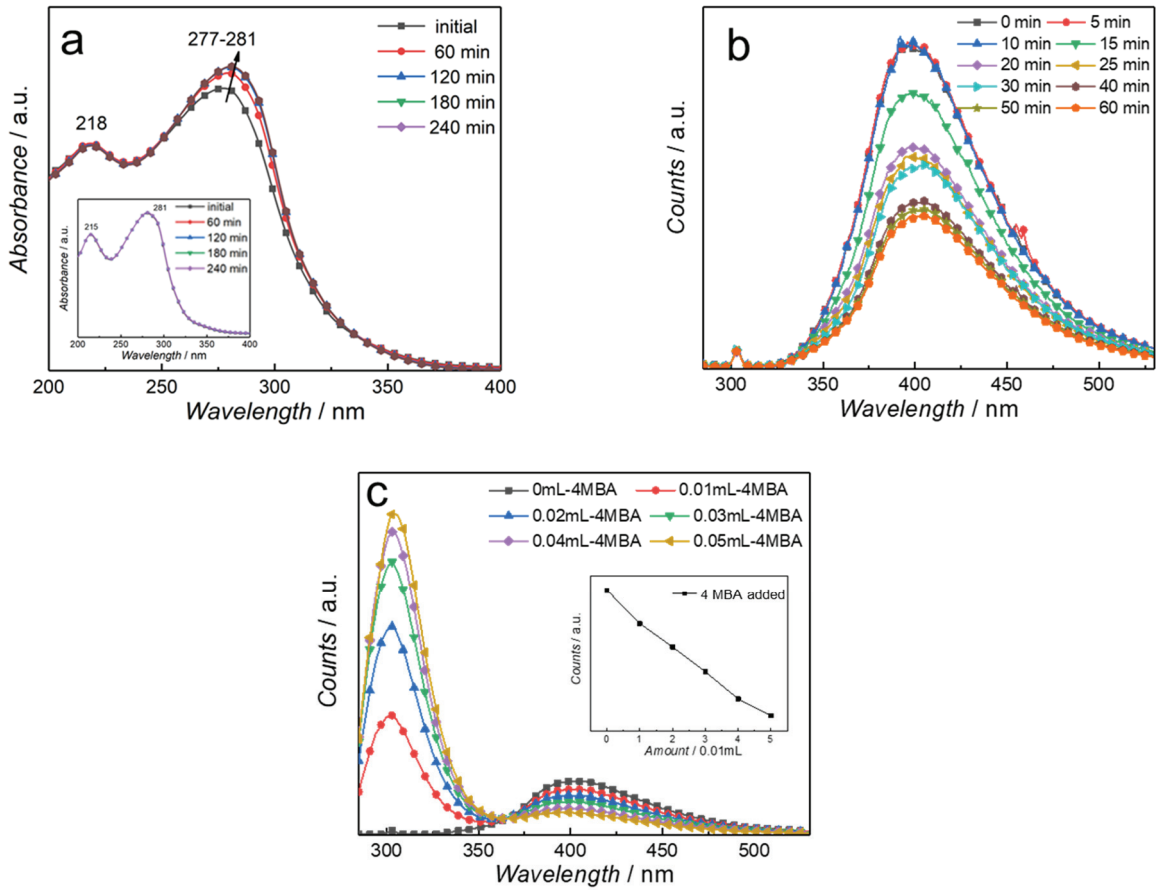

Figure 6. Spectroscopic studies. (a) in-situ UV-vis spectra of the K,Na-PHI in H_2O recorded during illumination at 365 nm under aerobic and O_2-free (inset) conditions. (b) in-situ steady-state emission spectra of K,Na-PHI recorded upon fluorescence excitation at 275 nm during external illumination at 365 nm every 5 min in water before (0-10 min) and after applying O_2 (10-60 min). (c) in-situ steady-state emission spectra of K,Na-PHI (λ_{ex} = 275 nm) dissolved in water with addition of 4MBA (5mM) during 365 nm illumination. The inset depicts the maximum intensity of the emission band at 402 nm (associated with KNa-PHI emission) upon addition of various amounts of 4MBA.

Conclusion

A facile low-temperature bottom-up synthesis of water-soluble heptazine-based polymeric carbon nitride exhibiting high photocatalytic activity and selectivity is reported for the first time. The excellent stability of colloidal solutions of K,Na-poly(heptazine imide) is conditioned by a high negative surface charge, a water solvation layer, and decreased number of terminal NH_x-groups as compared to bulk PCN, which precludes hydrogen-bonding between the heptazine units. The

water-soluble photocatalyst can be applied as an efficient dual-product selective photocatalyst for simultaneous benzylic alcohols oxidation and H_2O_2 production via reduction of dioxygen, exhibiting a 6.5 times higher reaction rate as compared to the conventional PCN. Moreover, the dissolved photocatalyst can be easily separated from the reaction medium by increasing the ionic strength of the solution, and repeatedly used in consecutive reaction cycles without any change in particle size and without any noticeable loss in activity or selectivity. This work thus establishes a new paradigm of easily operable *quasi*-homogeneous photocatalysis with carbon nitrides and paves the way for the use of water-soluble carbon nitrides in applications in which liquid aqueous processing or operation is mandatory.

Experimental procedures

The solid-state potassium poly(heptazine imide) (K-PHI-S) and water-soluble nanoparticles of mixed sodium-potassium poly(heptazine imide) (K,Na-PHI) were prepared by grinding 1.5 g of melamine with appropriate quantities of KOH or a mixture of KOH-NaOH and heating it in a lid-covered crucible at a rate of 5 °C min^{-1} up to 330 °C, then it was kept for 2h at the reached temperature before being withdrawn from the furnace. The obtained solid was powdered, dissolved in deionized water and dialysed yielding the nanoparticles solution in H_2O.

For the details on materials, synthesis, characterization, photocatalytic studies and the computational approach see the Supporting Information.

Acknowledgements

This work was funded by the Deutsche Forschungsgemeinschaft (DFG, German Research Foundation) – Projektnummer 364549901 – TRR 234 [Projects B6, B7, C3 and Z2] and BE 5102/3-1. We acknowledge also support by Spanish MINECO (MAT2016-78155-C2-1-R) and Gobierno del Principado de Asturias (GRUPIN-ID2018-170), and the project CICECO-Aveiro Institute of Materials, FCT Ref. UID/CTM/50011/2019, financed by national funds through the FCT/MCTES. L.M., M.S. and M.I. also acknowledge FCT/MCTES for funding (Project PTDC/QEQ-QAN/6373/20143). B.K. acknowledges the University of Iceland Research Fund for support through a PhD fellowship. Computational resources were provided by the state of Baden–

Württemberg through bwHPC and the German Science Foundation (DFG) under Grant No. INST 40/467-1 FUGG. C.N and A.T. acknowledge financial support of the DFG through the project TU 149/8-2 "Towards photo-active membranes for artificial photosynthesis" as well as the DFG through a research infrastructure grant INST 275/257-1 FUGG.

Conflict of interests

The authors declare no competing interests.

References

[1] X. Wang, K. Maeda, A. Thomas, K. Takanabe, G. Xin, J. M. Carlsson, K. Domen, M. Antonietti, *Nat. Mater.* **2008**, *8*, 76.

[2] a) P. Niu, L. Zhang, G. Liu, H. Cheng, *Adv. Funct. Mater.* **2012**, *22*, 4763-4770; b) Song, T. Lin, L. Lin, S. Lin, F. Fu, X. Wang, L. Guo, *Angew. Chem. Int. Ed.* **2016**, *55*, 2773-2777.

[3] a) Y. Ishida, L. Chabanne, M. Antonietti, M. Shalom, *Langmuir* **2014**, *30*, 447-451; b) Q. Cui, J. Xu, X. Wang, L. Li, M. Antonietti, M. Shalom, *Angew. Chem. Int. Ed.* **2016**, *55*, 3672-3676.

[4] a) S. Yang, Y. Gong, J. Zhang, L. Zhan, L. Ma, Z. Fang, R. Vajtai, X. Wang, P. Ajayan, *Adv. Mater.* **2013**, *25*, 2452-2456; b) K. Schwinghammer, M. Mesch, V. Duppel, C. Ziegler, J. Senker, B. Lotsch, *J. Am. Chem. Soc.* **2014**, *136*, 1730-1733.

[5] I. Krivtsov, E. Garcia-Lopez, G. Marci, L. Palmisano, Z. Amghouz, J. Garcia, S. Ordonez, E. Diaz, *Appl. Catal. B: Environ.* **2017**, *204*, 430-439.

[6] Z. Zhou, J. Wang, J. Yu, Y. Shen, Y. Li, A. Liu, S. Liu, Y. Zhang, *J. Am. Chem Soc.* **2015**, *137*, 2179-2182.

[7] C. Huang, J. Wen, Y. Shen, F. He, L. Mi, Z. Gan, J. Ma, S. Liu, H. Ma, Y. Zhang, *Chem. Sci.* **2018**, *9*, 7912-7915.

[8] Y. Zhang, Z. Zhou, Y. Shen, Q. Zhou, J. Wang, A. Liu, S. Liu, Y. Zhang, *Acs Nano* **2016**, *10*, 9036-9043.

[9] M. Groenewolt, M. Antonietti, *Adv. Mater.* **2005**, *17*, 1789-1792.

[10] a) Y. Li, S. Ouyang, H. Xu, X. Wang, Y. Bi, Y. Zhang, J. Ye, *J. Am. Chem. Soc.* **2016**, *138*, 13289-13297; b) Y. Li, P. Li, J. Wang, Y. Yang, W. Yao, Z. Wei, J. Wu, X. Yan, X. Xu, Y. Liu, Y. Zhu, *Appl. Catal. B:Environ.* **2018**, *225*, 519-529; c) B. Yuan, Z. Chu, G. Li, Z. Jiang, T. Hu, Q. Wang, C. Wang, *J. Mater. Chem. C* **2014**, *2*, 8212-8215.

[11] a) L. Heymann, S. Bittinger, C. Klinke, *Acs Omega* **2018**, *3*, 17042-17048; b) L. Heymann, B. Schiller, H. Noei, A. Stierle, C. Klinke, *Acs Omega* **2018**, *3*, 3892-3900.

[12] H. Ou, P. Yang, L. Lin, M. Anpo, X. Wang, *Angew. Chem. Int. Ed.* **2017**, *56*, 10905-10910.

[13] W. Wang, J. C. Yu, Z. Shen, D. K. L. Chan, T. Gu. *Chem. Comm.* **2015**, *50*, 10148-10150.

[14] J. Zhou, Y. Yang, C. Zhang, *Chem. Comm.* **2013**, *49*, 8605-8607.

[15] M. Stucchi, S. Cattaneo, A. Capella, W. Wang, D. Wang, A. Villa, L. Pratti. *Catal. Today* **2019** In press, **10.1016/j.cattod.2019.03.022**.

[16] a) E. Wirnhier, M. Doblinger, D. Gunzelmann, J. Senker, B. Lotsch, W. Schnick, *Chem. Eur. J.* **2011**, *17*, 3213-3221; b) D. Dontsova, S. Pronkin, M. Wehle, Z. Chen, C. Fettkenhauer, G. Clavel, M. Antonietti, *Chem. Mater.* **2015**, *27*, 5170-5179; c) V. Lau, I. Moudrakovski, T. Botari, S. Weinberger, M. Mesch, V. Duppel, J. Senker, V. Blum, B. Lotsch, *Nat. Comm.* **2016**, *7*.

[17] H. Yu, R. Shi, Y. Zhao, T. Bian, Y. Zhao, C. Zhou, G. Waterhouse, L. Wu, C. Tung, T. Zhang, *Adv. Mater.* **2017**, *29, 1605148*.

[18] a) A. Savateev, S. Pronkin, M. Willinger, M. Antonietti, D. Dontsova, *Chem. Asian J.* **2017**, *12*, 1517-1522; b) G. Zhang, L. Lin, G. Li, Y. Zhang, A. Savateev, S. Zafeiratos, X. Wang, M. Antonietti, *Angew. Chem. Int. Ed.* **2018**, *57*, 9372-9376.

[19] A. Savateev, S. Pronkin, J. Epping, M. Willinger, C. Wolff, D. Neher, M. Antonietti, D. Dontsova, *ChemCatChem* **2017**, *9*, 167-174.

[20] a) N. El-Gamel, L. Seyfarth, J. Wagler, H. Ehrenberg, M. Schwarz, J. Senker, E. Kroke, *Chem. Eur. J.* **2007**, *13*, 1158-1173; b) L. Seyfarth, J. Sehnert, N. El-Gamel, W. Milius, E. Kroke, J. Breu, J. Senker, *J. Mol. Struct.* **2008**, *889*, 217-228.

[21] a) E. Horvath-Bordon, E. Kroke, I. Svoboda, H. Fuess, R. Riedel, S. Neeraj, A. Cheetham, *Dalton Trans.* **2004**, *0*, 3900-3908; b) E. Horvath-Bordon, E. Kroke, I. Svoboda, H. Fuess, R. Riedel, *New J. Chem.* **2005**, *29*, 693-699.

[22] Y. Zhang, A. Thomas, M. Antonietti, X. Wang, *J. Am. Chem. Soc.* **2009**, *131*, 50-51.

[23] a) F. Su, S. Mathew, G. Lipner, X. Fu, M. Antonietti, S. Blechert, X. Wang, *J. Am. Chem. Soc.* **2010**, *132*, 16299-16301; b) X. Li, J. Chen, X. Wang, J. Sun, M. Antonietti, *J. Am. Chem. Soc.* **2011**, *133*, 8074-8077; c) M. Zhou, P. Yang, S. Wang, Z. Luo, C. Huang, X. Wang, *ChemSusChem* **2018**, *11*, 3949-3955; d) A. Savateev, D. Dontsova, B. Kurpil, M. Antonietti, *J. Catal.* **2017**, *350*, 203-211; e) A. Savateev, I. Ghosh, B. Konig, M. Antonietti, *Angew. Chem. Int. Ed.* **2018**, *57*, 15936-15947.

[24] I. Krivtsov, M. Ilkaeva, E. Garcia-Lopez, G. Marci, L. Palmisano, E. Bartashevich, E. Grigoreva, K. Matveeva, E. Diaz, S. Ordonez, *ChemCatChem* **2019**, *11*, 2713-2724.

[25] a) Y. Shiraishi, S. Kanazawa, Y. Sugano, D. Tsukamoto, H. Sakamoto, S. Ichikawa, T. Hirai, *Acs Catal.* **2014**, *4*, 774-780; b) Y. Shiraishi, Y. Kofuji, H. Sakamoto, S. Tanaka, S. Ichikawa, T. Hirai, *Acs Catal.* **2015**, *5*, 3058-3066; c) A. Torres-Pinto, M. Sampaio, C. Silva, J. Faria, A. Silva, *Appl. Catal. B:Environ.* **2019**, *252*, 128-137; d) M. Ilkaeva, I. Krivtsov, J. Garcia, E. Diaz, S. Ordonez, E. Garcia-Lopez, G. Marci, L. Palmisano, M. Maldonado, S. Malato, *Catal. Today* **2018**, *315*, 138-148.

[26] L. Sun, J. Bolton, *J. Phys. Chem.* **1996**, *100*, 4127-4134.

[27] D. Wakerley, M. Kuehnel, K. Orchard, K. Ly, T. Rosser, E. Reisner, *Nat. Energ.* **2017**, *2*, 17021.

[28] M. Ilkaeva, I. Krivtsov, E. Bartashevich, S. Khainakov, J. Garcia, E. Diaz, S. Ordonez, *Green Chem.* **2017**, *19*, 4299-4304.

Graphical abstract

Water-soluble colloidal nanoparticles of polymeric carbon nitride enable *quasi*-homogeneous photocatalysis with unprecedented performance. The dissolved photocatalyst can be easily recovered and re-dissolved by simple modulation of the ionic strength of the medium, retaining its excellent activity and selectivity.

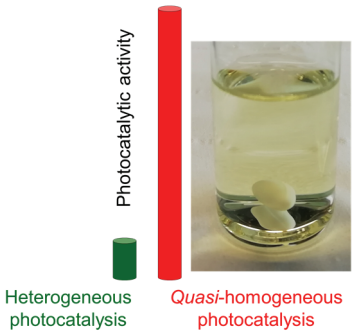

Keywords

Photocatalysis, Nanoparticles, Carbon Nitride, Chemoselectivity, Reusability

SUPPORTING INFORMATION

Water-soluble polymeric carbon nitride colloidal nanoparticles for highly selective *quasi*-homogeneous photocatalysis

by Krivtsov et al.

Experimental Procedures

Materials and synthesis

Melamine (99 %) provided by Sigma Aldrich, KOH and NaOH (Merck, 99 %) were used for the syntheses of the photocatalysts. 4-methoxybenzyl alcohol (4MBA), 4-methoxybenzaldehyde (4MBAL) both with purity of 98% were supplied by Sigma Aldrich and used for the photocatalytic tests. Titanium oxysulfate hydrate containing approx. 17 wt% of sulfuric acid ($TiOSO_4 \cdot H_2O \cdot H_2SO_4$) and aqueous solution of H_2O_2 were purchased from Sigma Aldrich and used for photometric determination of H_2O_2.Conventional heptazine-based polymeric carbon nitride (CN) was synthesized for comparison by thermal condensation of 30 g of melamine at 530 °C for 4h, after that the solid was powdered in agate mortar. The solid-state potassium poly(heptazine imide) (K-PHI-S) and water-soluble nanoparticles of potassium poly(heptazine imide) (K-PHI), sodium poly(heptazine imide) (Na-PHI), and mixed sodium-potassium poly(heptazine imide) (K,Na-PHI) were prepared by grinding 1.5 g of melamine with appropriate quantities of KOH, NaOH or a mixture of KOH-NaOH and heating it in a lid-covered crucible at a rate of 5 °C min^{-1} up to 330 °C, then it was kept for 2h at the reached temperature before being withdrawn from the furnace. The obtained solid was powdered and mixed with 100 mL of deionized water. In the case of the K-PHI-S sample, the suspended solid was centrifuged and washed twice with deionized H_2O before being put inside a cellulose membrane with a pore size of 3.5 kDa and dialyzed against H_2O for the purification followed by drying it for 24 h at 80 °C. For the preparation of the K-PHI, Na-PHI and K,Na-PHI samples, the same procedure was implemented with the difference that after the addition of 100 mL of H_2O the insoluble part was filtered out, firstly, by a paper filter and then by a 0.2 μm PTFE syringe filter. Eventually, the solution of the alkali metal poly(heptazine imide) nanoparticles was dialyzed and concentrated by evaporation at 60 °C to a concentration of 5 g L^{-1}, which was determined gravimetrically. In order to obtain solid sample of the water-soluble alkali metal poly(heptazine imide), the solution was gradually evaporated at 60 °C and then dried for 24 h at 80 °C. Table S1 summarizes the synthetic conditions applied for the preparation of the poly(heptazine imide) samples and the yields of the obtained materials.

Characterization

A Mettler–Toledo instrument (TGA/SDTA851^e) was used to investigate the formation of K,Na-PHI from the melamine mixture with KOH/NaOH. For this, a small portion of a precursor containing 1.5 g of melamine, 0.56 g (10 mmol) of KOH and 0.2 g of NaOH (5 mmol) was put in a platinum crucible and heated at a rate of 5 °C min^{-1} up to 330 °C in He atmosphere. Thermal decomposition of the dried alkali metal poly(heptazine imide) samples was carried out using the same equipment, but at a heating rate of 10 °C min^{-1} in O_2 flow (50 mL min^{-1}) from 25 °C to 1000 °C. XRD patterns were obtained using a Pananalytical X'pert PRO diffractometer equipped with a Pixel detector and operating at Cu Kα radiation. FTIR spectra were recorded by means of a Shimadzu IRTracer-100 spectrometer at a resolution of 4 cm^{-1} from the samples powdered and pressed into KBr pellets.

^1H, ^{13}C and ^{15}N magic angle spinning (MAS) solid-state NMR spectra of the K-PHI-S and the dried K,Na-PHI samples were acquired on a Bruker Avance III 400 spectrometer operating at B_0 field of 9.4 T with ^1H, ^{13}C, ^{15}N Larmor frequencies of 400.1/100.6/40.6 MHz, respectively. All experiments were performed on a double-resonance 4 mm Bruker MAS probe, except the ^{15}N cross-polarization MAS (CPMAS) measurements, in which a double-resonance 7 mm Bruker MAS probe was used. Samples were packed into 4 or 7 mm zirconia rotors. Spinning rates between 5 and 15 kHz were employed to record all spectra. ^1H, ^{13}C and ^{15}N chemical shifts are quoted in ppm from: TMS (0 ppm) and α-glycine (secondary reference, C=O at 176.03 ppm and NH_3^+ at 347.6 ppm on the nitromethane scale, respectively). Specifically, the ^{13}C NMR spectra were acquired using a high-power decoupling single pulse sequence with the following conditions: 12 kHz spinning rate, a pulse width of 2.56 μs (45° flip angle) corresponding to 49 kHz, with ^1H SPINAL-64 decoupling at 80 kHz, recycle delay (RD) was 60 s. The ^1H-^{13}C CPMAS spectra were acquired at 12 kHz MAS, ^1H 90° pulse set to 3.2 μs (78 kHz); the CP step was performed with a contact time (CT) of 3500 μs using a 50−100% RAMP shape pulse on the ^1H (66 kHz) channel and using a 45 kHz square pulse on the ^{13}C channel; RD was 5 s. During the acquisition, a SPINAL-64 decoupling

scheme was employed using a pulse length for the basic decoupling units of 6 μs at rf field strength of 80 kHz. ^{1}H-^{15}N CPMAS spectra were typically acquired with the following parameters: MAS 5 kHz, ^{1}H 90°pulse with a rf of 4 μs (63 kHz), the CP step was performed with a CT of 2000 μs using a 50−100% RAMP shape on the ^{1}H (57 kHz) channel and using a 34 kHz square shape pulse on the ^{15}N channel; decoupling with SPINAL-64 using a pulse length of 6.8 μs at rf field strength of 63 kHz was applied, RD was 5 s. All spectra were acquired at ambient probe temperature. MagicPlot Pro software was used for the deconvolution of the chosen spectra. The R^2 values for fitting curves were always higher than 0.97.

In order to perform X-ray photoelectron spectroscopy (XPS), the powder samples K-PHI-S and K,Na-PHI were placed on top of a conductive double-sided carbon tape (Ted Pella Inc., USA) and fixed to the XPS sample holder. The measurements were performed using a UHV Multiprobe system (Scienta Omicron, Germany) with a monochromatic X-ray source (Al Kα) and an electron analyzer (Argus CU) with 0.6 eV energy resolution. Charge compensation during data acquisition was realized by an electron flood gun (NEK 150, Staib, Germany) at 6 eV and 50 μA. The background was subtracted and spectra were calibrated using the C1s peak (284.6 eV) before undergoing fitting using Voigt functions (30:70). A scanning electron microscope JEOL-6610LV equipped with an Oxford Instruments EDX detector was used to collect SEM images of the dry poly(heptazine imide) samples and determine their elemental composition. Particle size distribution of the water-soluble poly(heptazine imide) samples and their zeta-potentials were determined by means of dynamic light scattering (DSL) and electrophoretic mobility methods using a Zetasizer Nano ZS (Malvern Instruments Ltd., UK) operating at a detection angle of 173.5°. Diffusive-reflectance UV-vis spectra of solids were taken by a Shimadzu UV2600 UV-vis spectrophotometer. UV-vis spectra of the poly(heptazine imide) nanoparticles solutions were recorded using a Cary 60 (Agilent Technologies) spectrophotometer. Cyclic voltammogram of the K,Na-PHI material was recorded in the dark in acetonitrile solution of tetrabutylammonium hexafluorophosphate ($TBAFP_6$, 0.1 M) using a SP-300 BioLogic potentiostat (Caix, France) and a three-electrode cell composed of a platinum counter electrode and an Ag/AgCl (sat. KCl) reference electrode. The working electrode was prepared by drop casting of the K,Na-PHI nanoparticles solution on a glassy carbon substrate followed by gelation by adding conc. HCl. The potential values were recalculated and reported with respect to the normal hydrogen electrode (NHE). The images were recorded using the SALVE at 80kV acceleration voltage (where indicated) and the Philips CM20 at 200kV, both in HRTEM mode. The liquid sample was diluted (where indicated) in purified water (10 μl of sample in 1 mL of water), then drop cast onto copper TEM support grids with holey carbon film. The undiluted liquid samples were prepared by dipping of the TEM grid into the solution and drying. The solid samples were sonicated in ethanol and then drop cast onto TEM grids.

Photocatalytic measurements

Selective photocatalytic oxidation of 4MBA to 4MBAL was carried out for the K-PHI-S, K-PHI, Na-PHI, and K,Na-PHI samples, CN was used as a reference. For this purpose, the solid samples and the solutions of the poly(heptazine imide) nanoparticles were suspended in 20 mL of water or water-acetonitrile solution of 4MBA (0.1 mmol). The pH of water solutions or water-acetonitrile mixture was in the range of 6.5–7.0 and did not undergo noticeable changes after irradiation. The reaction mixture was irradiated for 4 h by a UV LED emitting at 365 nm and producing a photon flux of 40 mW cm^{-2}. The samples of 0.1 mL were taken every 30 min and analyzed by an HPLC Shimadzu LC-10ADvp equipped with a UV detector SPD-20A and a reversed phase C18 Nucleosil column. Acetonitrile/water (30/70 vol.) was used as a mobile phase at a flow of 1.2 mL min^{-1} and a column temperature of 60 °C. 4MBA to 4MBAL were detected and quantified at a wavelength of 240 nm. Considering a quasi-homogeneous nature of the irradiated 4MBA solutions with the poly(heptazine imide) photocatalysts and the incompatibility of the used HPLC column with some of the organic solvent immiscible with water, which could possibly be used for the organic compounds extraction, the following probe preparation was implemented. The photocatalyst was separated from the reaction medium by means of a salting-out approach. In details, to 0.1 mL of the sample, 0.2 mL of 1M NaCl solution, and 0.8 mL of acetonitrile were added, the salting-out effect resulted

in the two-phase system with the photocatalyst in the aqueous phase and 4MBA, 4MBAL extracted to the organic phase, which was subsequently analysed. The respective volumes of the additives for the probe-preparation were adjusted for the case of acetonitrile/water solutions, as to maintain the H_2O to acetonitrile ratio in the probe constant. The calibration was carried out in the same way giving R^2 values higher than 0.999 for the substrate and the product. The recyclability test was made possible by the precipitation of the photocatalyst after each cycle by adding 0.25 g of NaCl to the reaction mixture in water solution and 0.125 to the reaction mixture in water/acetonitrile medium, following by its centrifugation and re-dispersion in a fresh solution of 4MBA. The selectivity (S) of the reaction was determined by the formula:

$$S_{4MBAL} = \frac{C(4MBAL)}{C_0(4MBA) - C(4MBA)} * 100\%,$$

where C_0(4MBA) is the initial concentration of the substrate, C(4MBA) is the substrate concentration at a given reaction time, and C(4MBAL) is the concentration of the reaction product at a given reaction time. Considering a *quasi*-homogeneous nature of the carried out photocatalytic reaction, the estimation of the quantum yield of the process is more reliable than for the case of heterogeneous systems. For this, the reaction mixture in water(60%)/acetonitrile(40%) medium containing 4MBA (5mM) and the K,Na-PHI photocatalyst having absorbance of 0.1 at 365 nm were put in a quartz cuvette and irradiated with a 365 nm emitting LED for 2 h. After the reaction the concentration of the produced 4MBAL was analysed using the above described HPLC method. The quantum yield (Q) of the process was calculated considering that two electrons are required to be withdrawn from the substrate (4MBA) to oxidize it to 4MBAL (1).

$$C_6H_3COH_3CH_2OH + 2h^+ \rightarrow C_6H_3COH_3CHO + 2H^+ \qquad (1)$$
$$O_2 + 2H^+ + 2e^- \rightarrow H_2O_2 \qquad (2)$$

The photon flux was determined by the formula:

$$\Phi = \frac{\Delta H}{qE},$$

where ΔH is the light power absorbed by the system (W m^{-2}), q is the charge of electron (C) and E is the energy of irradiation (eV).

The quantum yield was determined as:

$$\mathrm{Q} = \frac{2\ \mathrm{n(4MBAL)}\ N_A}{\Phi t S},$$

where n(4MBAL) is the number of moles of 4MBAL produced, N_A is the Avogadro number, t is the irradiation time in s, and S is the irradiated area of the reactor (m^2)

Hydrogen peroxide concentration was estimated photometrically. Sample of 5 mL of the reaction solution was withdrawn after 4 h of irradiation, to that volume 1 mL of $TiOSO_4$ solution (Ti 1 wt%) in sulfuric acid was added. The addition of the acidic solution caused the photocatalyst to coalesce, so it could be filtered out through the syringe PTFE 0.2 µm filter. The filtered solution of yellow-coloured titanium peroxocomplex was analysed photometrically using a Cary 60 (Agilent Technologies) spectrophotometer. The absorption at 420 nm was chosen to plot a calibration curve using standard H_2O_2 concentrations and to estimate the concentrations of photocatalytically produced H_2O_2. The selectivity towards the H_2O_2 formation was determined by the formula:

$$S_{H_2O_2} = \frac{C(H_2O_2)}{C_0(4MBA) - C(4MBA)} * 100\%.$$

Theoretical calculations

Periodic Density Functional Theory (DFT) calculations were performed using the Vienna *Ab initio* Simulation Package (VASP) version 5.4.4[1–4] using the projector-augmented wave method[5] to represent the basis set. The exchange-correlation functional by Perdew, Becke, and Ernzerhof was used.[6] The wavefunction was optimized to an accuracy of 10^{-6} eV while geometries were relaxed until the forces reached below $5 \cdot 10^{-2}$ eV $Å^{-1}$. Gaussian finite-temperature smearing was employed with a smearing width of 0.01 eV. A plane wave energy cut-off of 400 eV and a 2x4x1 Monkhorst-Pack[10] ***k*** grid were found to give converged total energy results. 20 Å of vacuum separated slabs in *z* direction to avoid interaction between periodic images. For implicit solvation calculations, the GLSSA13 solvent model[7] implemented in the VASPsol extension was invoked.[8,9] We assumed typical room temperature bulk solvent dipole moments of 78.4, 36.6, and 32.6 for water, acetonitrile, and methanol, respectively.

Spectroscopic studies

In situ UV-Vis absorption and emission spectra were acquired in a 1cm quartz cell using a JASCO V-780 spectrophotometer and a fluorescence spectrometer (FLS980, Edinburgh), respectively. The data were recorded at room temperature upon irradiation of the sample with at 365 nm. External irradiation with the irradiance of 71 mW / mm^2 at the sample position was provided by a combined mounted LED (M365LP1, THORLABS). The K,Na-PHI sample was diluted in H_2O giving the optical density below 0.8 at 280 nm, and the freeze−pump−thaw method was used to remove oxygen for the measurements.

Results and Discussion

Synthesis

Table S1. Synthetic conditions for the poly(heptazine imide) samples preparation.

Sample name[a]	Melt composition	Sample state	Yield[c]	XRD phase composition[d]
		Potassium poly(heptazine imide)		
K-PHI-S1	KOH 5 mmol (0.28 g)	Mostly solid	27 %	PHI and melamine
K-PHI-S2	KOH 7.5 mmol (0.42 g)	Mostly solid	29 %	PHI and melamine
K-PHI-S3	KOH 10 mmol (0.56 g)	Solid and soluble PHI	23-26 %	PHI and melamine
K-PHI-S	KOH 10 mmol (0.56 g)	Dialyzed solid	24-25 %	PHI
K-PHI	KOH 12.5 mmol (0.70 g)	Dialyzed solution	10-11 %	PHI
K-PHI4	KOH 15 mmol (0.84 g)	Dialyzed solution	9 %	PHI
K-PHI5	KOH 20 mmol (1.12 g)	Dialyzed solution	3 %	PHI
		Sodium poly(heptazine imide)		
Na-PHI	NaOH 5 mmol (0.2 g)	Dialyzed solution	13 %	PHI
Na-PHI1	NaOH 7.5 mmol (0.3 g)	Dialyzed solution	4 %	PHI
Na-PHI2	NaOH 10 mmol (0.4 g)	Dialyzed solution	negligible	
		Potassium-Sodium poly(heptazine imide)		
K,Na-PHI1	KOH 5 mmol (0.28 g) NaOH 5 mmol (0.2 g)	Dialyzed solution	6-9 %	PHI
K,Na-PHI2	KOH 7.5 mmol (0.42 g) NaOH 7.5 mmol (0.3 g)	Dialyzed solution	12-18 %	PHI
K,Na-PHI3	KOH 10 mmol (0.56 g) NaOH 10 mmol (0.4 g)	Dialyzed solution	9-11 %	PHI
K,Na-PHI4	KOH 10 mmol (0.56 g) NaOH 7.5 mmol (0.3 g)	Dialyzed solution	7-9 %	PHI
K,Na-PHI	KOH 10 mmol (0.56 g) NaOH 5 mmol (0.2 g)	Dialyzed solution	31-42 %	PHI

[a] The samples highlighted in grey are chosen for the investigation. [b] The materials were prepared by grinding 1.5 g of melamine with appropriate quantities of KOH, NaOH or a mixture of KOH-NaOH and heating it in a lid-covered crucible at a rate of 5 °C min^{-1} up to 330 °C, then it was kept for 2 h at the reached temperature before being withdrawn from the furnace. [c] The yield was quantified as the mass of the solid obtained after the synthesis (after washing or after dialysis) to the mass of melamine used for the synthesis and multiplied by 100 %. The yields depend on the presence of absorbed moisture in the hydroxide, hence may vary significantly [d] XRD patterns were collected from the dry solid samples, (PHI corresponds to alkali metal poly (heptazine imide) phase).

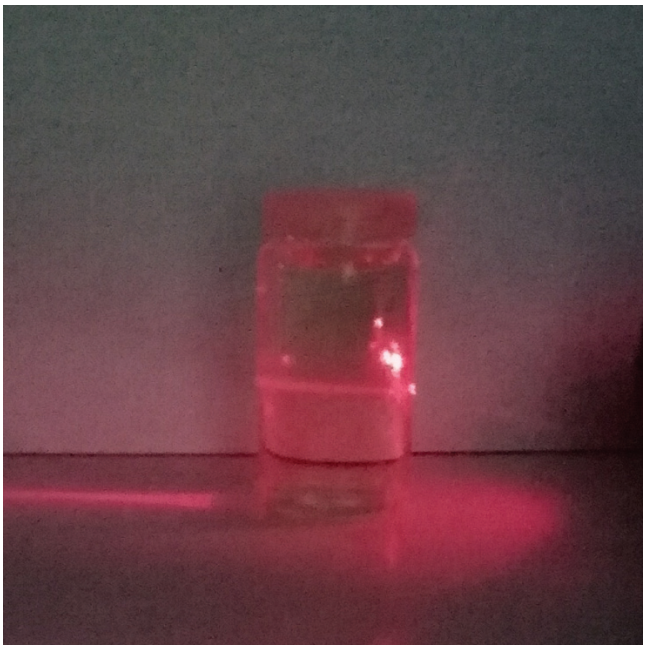

Figure S1. Tyndall effect observed in the solution of K,Na-PHI nanoparticles

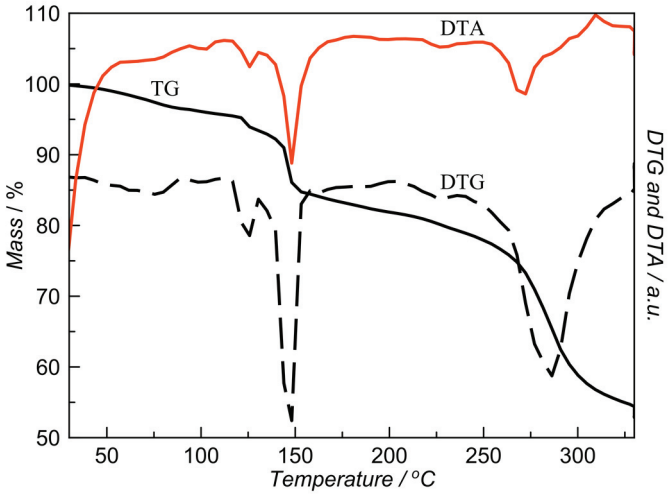

Figure S2. TG, DTG and DTA curves corresponding to the condensation process of melamine in KOH/NaOH mixture under He flow.

XRD analysis

The XRD patterns of the K-PHI-S sample series, obtained at different loadings of KOH in the melt, show that a part of melamine present in the precursor does not undergo the condensation to carbon nitride polymers, which is due to the fact that KOH is solid in this temperature range and it does not provide a liquid medium for melamine dissolution and condensation (Fig. S3 Left). Although the material recovered after the synthesis in KOH (K-PHI-S) was insoluble in water, its purification by washing and centrifugation or filtering was complicated owing to its high dispersibility in it. This is why the solid was dialysed, which allowed to achieve its higher purity (Fig. S3 Left).

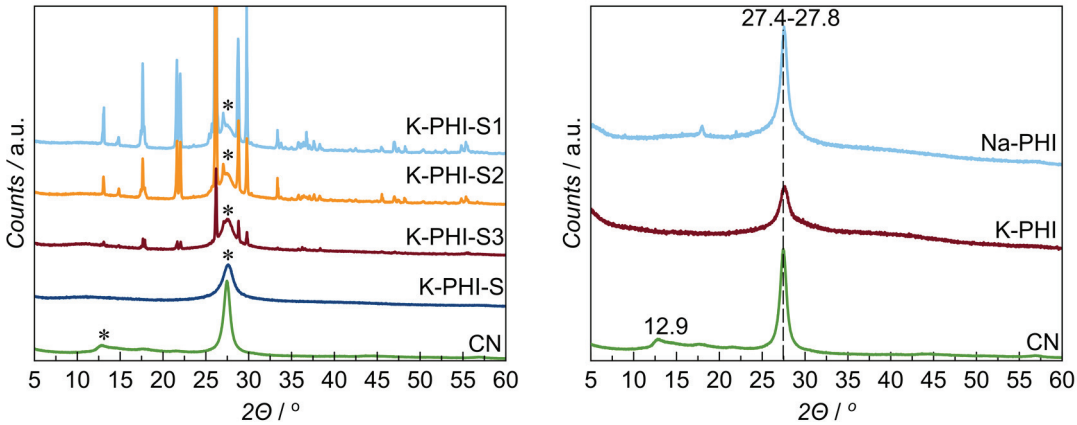

Figure S3. XRD patterns of the K-PHI-S samples (left) and the water soluble K-PHI and Na-PHI samples (right). Asterisk indicates the poly(heptazine imide) or PCN phases, while the other peaks correspond to non-condensed melamine.

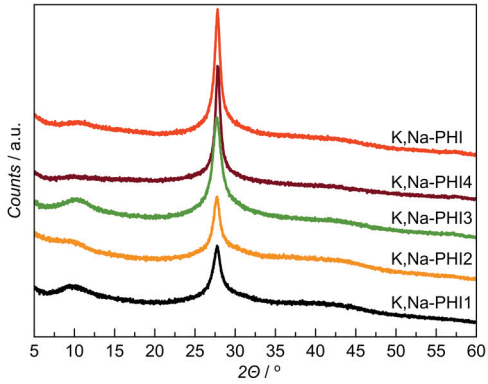

Figure S4. XRD patterns of the K,Na-PHI samples.

FTIR analysis

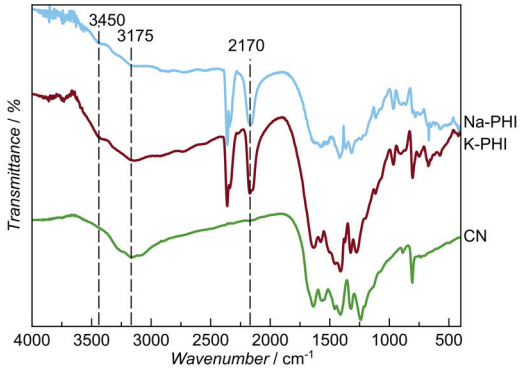

Figure S5. FTIR spectra of the K-PHI and Na-PHI samples in comparison with the CN sample.

TG-DTA analysis

The maximum of thermal decomposition rate of the K-PHI-S and K,Na-PHI samples is observed at about 690 °C (Fig. S6). A clear difference of thermal behaviour of the studied materials could be seen at high-temperature range. K-PHI-S loses 100 % of its initial mass by 800 °C, which it is not the case of K,Na-PHI retaining about 18 % of its initial mass at the same temperature (Fig. S6). The decomposition of the samples might result in the formation of potassium and sodium carbonates, hydroxides or oxides which are all not volatile compounds, however they melt at temperatures above 800 °C and then can be carried away by the gas flow (Fig. S6).

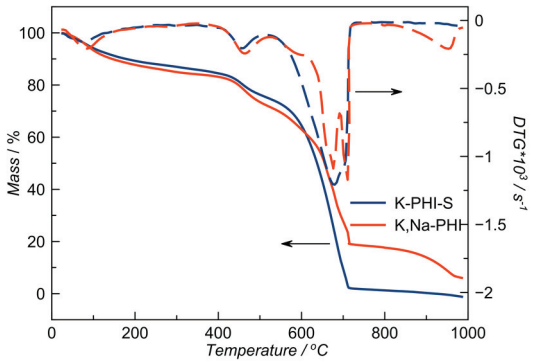

Figure S6. Thermoanalytical curves of the K-PHI-S and K,Na-PHI samples decomposition in O_2 (50 mL min^{-1}).

Elemental analyses

Table S2. Elemental composition of the prepared samples.

Sample name	Elemental composition / wt%[a]	C:N:H[a]	EDX Elemental composition / at% [b]	C:N ratio[b]
K-PHI-S	$C_{29.4}N_{50.5}H_{2.2}$	0.67:1.00:0.61	$C_{35.4}N_{56.1}O_{5.8}K_{2.7}$	0.63
K-PHI	-		$C_{35.6}N_{51.3}O_{8.6}K_{4.5}Ca_{0.1}$	0.69
Na-PHI	-		$C_{33.3}N_{54.2}O_{8.5}Na_{3.8}Ca_{0.2}$	0.61
K,Na-PHI	$C_{27.0}N_{44.4}H_{1.8}$	0.72:1.00:0.56	$C_{34.9}N_{47.8}O_{11.2}K_{2.5}Na_{3.5}Ca_{0.2}$	0.73

[a] On the basis of CHN elemental analysis. [b] Obtained by SEM-EDX method.

NMR study

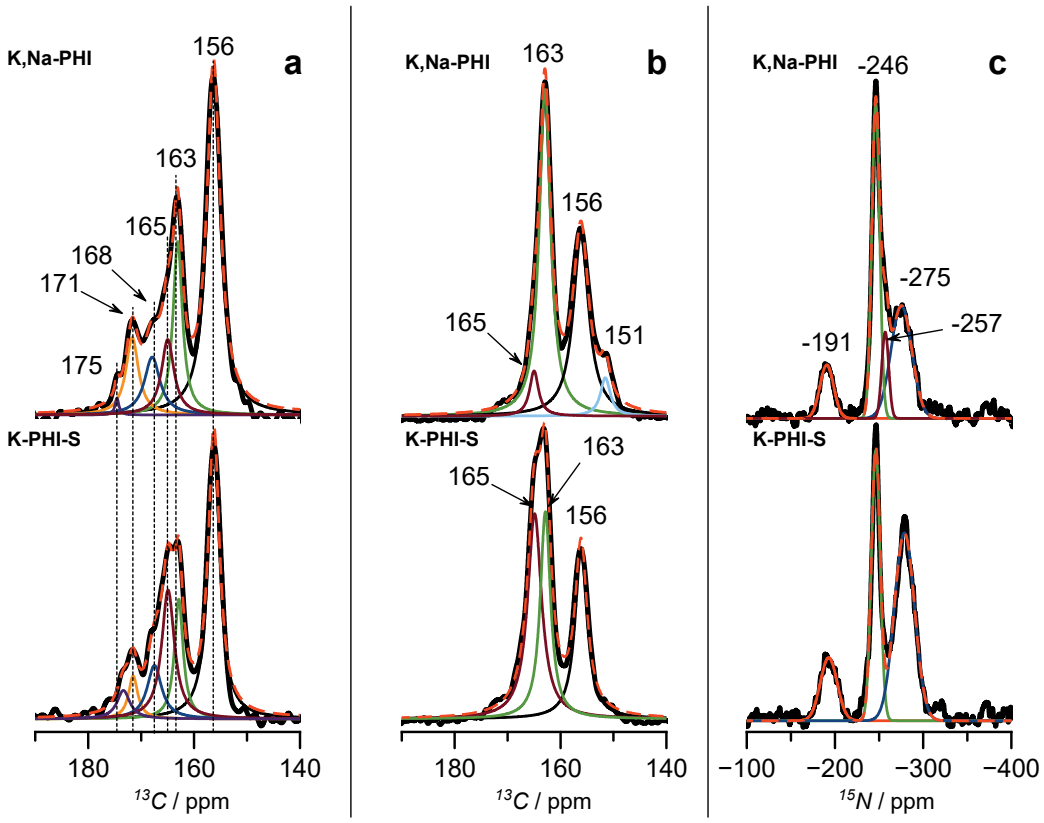

Figure S7. Peak fitting of the a) ^{13}C direct excitation MAS, b) ^{1}H-^{13}C CPMAS, and c) ^{1}H-^{15}N CPMAS solid-state NMR spectra of the K-PHI-S and K,Na-PHI samples. The experimental and fitted curves are represented in solid black and dashed red lines, respectively.

The ^{13}C direct excitation MAS spectra provide a quantitative estimation of the PCN species present in the studied samples (Table S3 and Fig. S7). The peak area of resonance **3** (associated to poly(heptazine) units) is used to estimate the relative amount of nitrile, C≡N (**1**), secondary amines, N=C-NH (**4**), primary amines, N=C-NH_2 (**5**), and oxygenated functional groups, N=C-O^- (**6**), between samples K,Na-PHI and K-PHI-S, by taking the ratios **1:3**, **4:3**, **5:3** and **6:3,** respectively (Table S3). The **6:3** ratio is similar in both materials (*cf.* 0.20 *vs.* 0.24) indicating that the relative amount of the C-O^- species is nearly identical for both. In contrast, the number of -NH_2 groups (**5:3** ratio) in the water-soluble K,Na-PHI decreases with respect to K-PHI-S (*cf.* 0.20 *vs.* 0.50, respectively), suggesting that the KOH/NaOH medium promotes a higher degree of condensation of the -NH_2 groups. Consequently, the formation of heptazine species (Fig. S8) is favoured, resulting in an increased number of N-C=N (**3**) carbons in K,Na-PHI as compared to K-PHI-S (Table S3, Fig. S7). The lower concentration of terminal -NH_2 moieties in K,Na-PHI will likely lead to an overall decrease of the number of hydrogen bonds in the polymer network, thus exerting a direct influence on aggregation and solubility.

Table S3. Estimation of relative concentrations of the PCN species from the deconvoluted ^{13}C MAS NMR spectra

Peak position	Assignment	Contribution of the peak area to the total area of the spectrum (FWHM)		Peak area ratio of the peaks with respect to the area of **3**	
		K-PHI-S	K,Na-PHI	K-PHI-S	K,Na-PHI
122 (**1**)	C≡N	0.13 (6.6)	0.15 (6.6)	0.34	0.35
156 (**3**)	N=C-N (C-N_3)	0.38 (2.6)	0.43 (3.0)	1	1
163 (**4**)	N=C-NH	0.12 (2.0)	0.15 (2.1)	0.32	0.35
165 (**5**)	N=C-NH_2	0.19 (2.9)	0.09 (2.9)	0.50	0.20
168 (**6**)	N=C-O^-	0.09 (3.3)	0.08 (3.5)	0.24	0.20
171-175 (**7**)	C-N^-	0.09 (2.1+2.9)	0.10 (2.9+1.0)	0.24	0.23

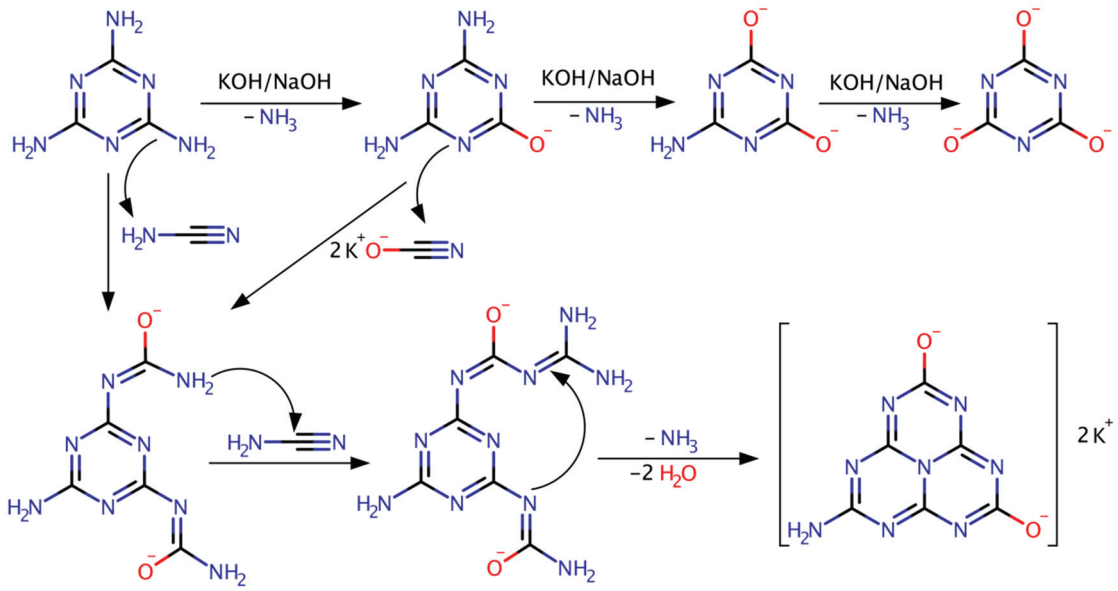

Figure S8. Proposed poly(heptazine imide) condensation pathway in KOH/NaOH melt.

XPS study

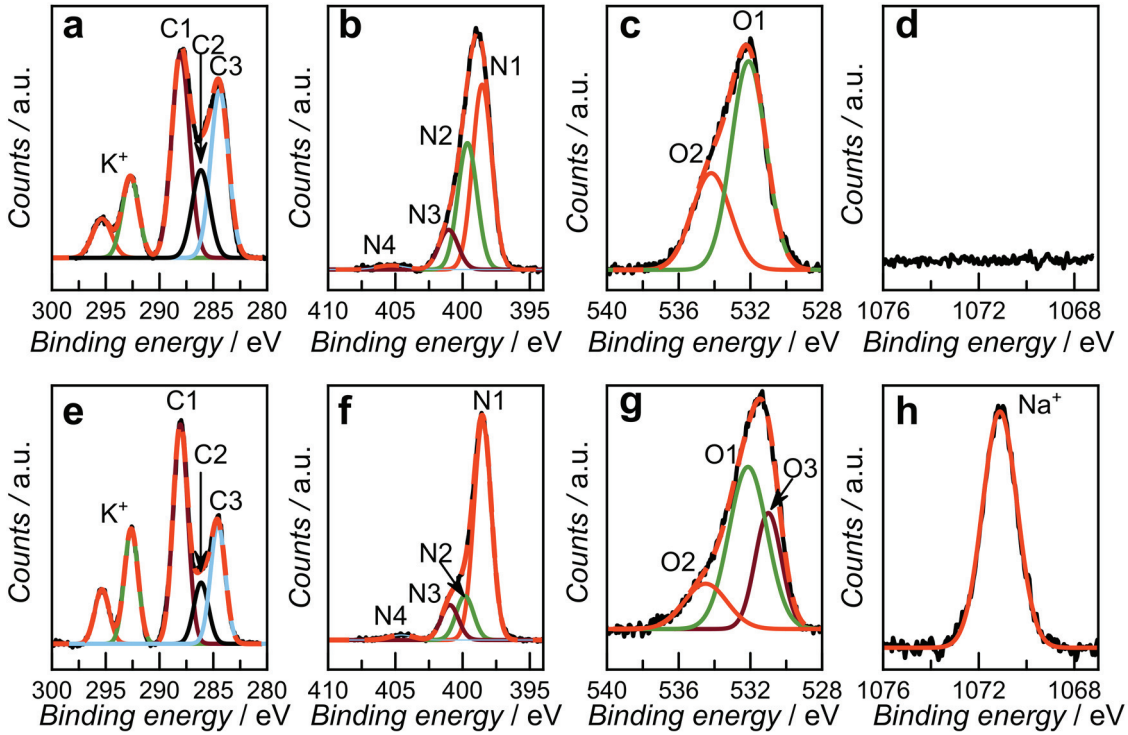

Figure S9. (a, b, c, d) and (e, f, g, h) XP C1s, N1s, O1s and Na1s spectra obtained for the K-PHI-S and K,Na-PHI samples, respectively.

Table S4. XPS data analysis.

Peak	Assignment	Peak position / eV	
		K-PHI-S	K,Na-PHI
C1	N-C=N, C=O	288.0	288.1
C2	C-OH, C-NH_2	286.2	286.1
C3	C-C from carbon tape and adventitious carbon	284.4	284.6
N1	C-N=C, C≡N	398.5	398.5
N2	N-C_3, triazine C-NH_x*	399.6	399.8
N3	C-NH_x	401.0	400.9
N4	N-N	405.3	405.4
O1	O=C-O	532.1	532.1
O2	H_2O	534.2	534.5
O3	HCO_3^-	-	531.0
Ratio between the areas corresponding to the N1:N2:N3 species			
		1:0.68:0.21	1:0.20:0.16

*Peak N2 cannot be assigned solely to the N-C_3 groups, since the ratio between the peak areas of N2:N1 in the K-PHI-S sample of 0.68:1 is far superior to the theoretically possible for the fully condensed polyheptazine structure (*ca.* 0.16:1). We attribute this peak also to the contribution from -NH_x bearing triazine fragments such as melamine.[11,12]

Theoretical study of K,Na-PHI

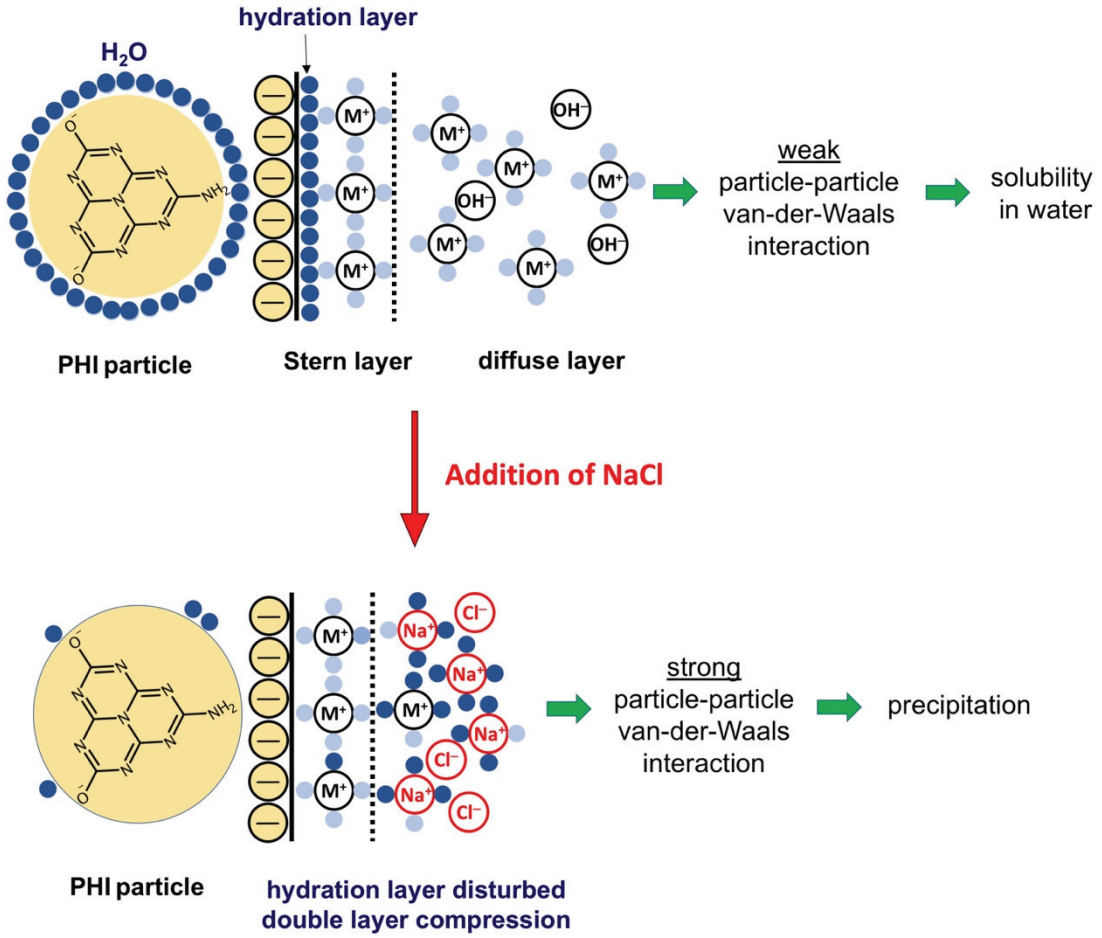

Figure S10. The salting out effect of NaCl addition on the double layer of the K,Na-PHI nanoparticles and their subsequent precipitation. At low ionic strength, the surface of PHI particles is covered with a hydration layer of water molecules, and the electric double layer extends over a relatively large distance, making the inter-particle van-der-Waals attractive forces weak. With increasing Na^+ concentration, due to the addition of NaCl, the hydration layer will gradually be stripped, disturbed as the water molecules hydrate preferentially the Na^+ cations; at the same time, the double layer is compressed due to the more effective screening by Na^+ ions. These effects result in stronger attractive particle-particle van-der-Waals interaction, leading to the coalescence of K,Na-PHI nanoparticles and their precipitation. The process is reversible: after centrifugation and removal of concentrated NaCl solution, the addition of water yields the PHI colloidal particles fully soluble again. M^+ stands for Na^+ or K^+.

The model system used for calculations is shown in Fig. S11 and is based on our experimental characterization; it exhibits a higher degree of condensation than typical carbon nitride model systems based on a periodic arrangement of melon strings but leaves enough boundaries to accommodate some functional groups to represent different N or O containing moieties.

Results of the solvation stabilisation study using the GLSSA13 implicit solvation model are summarized in Table S5. The stability of the model system in water, acetonitrile, and methanol is compared. Two main trends can be extracted from this data: (i) the water environment appears to stabilise the model system more strongly than the other two polar solvents, and (ii) stabilisation improves as a function of the number of oxygen-containing moieties.

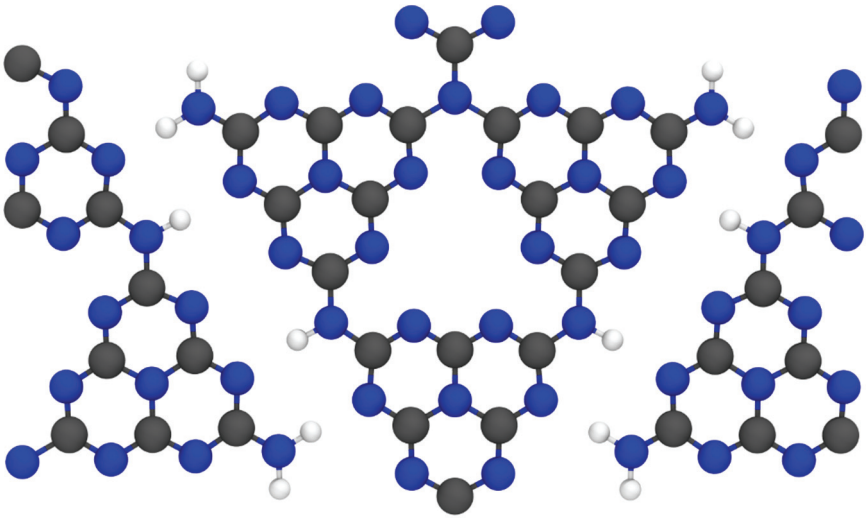

Figure S11. Illustration of one unit cell of the periodic computational carbon nitride model employed in the DFT study. The four -NH_2 groups are subsequently exchanged for -OH for the solvation study.

Table S5. Stabilisation of the carbon nitride model system in different implicit solvent models.

	Stabilization / eV vs. gas phase		
# of NH_2 exchanged	in water	in ACN	in MeOH
0	-1.46	-1.14	-1.10
1	-1.57	-1.24	-1.19
2	-1.66	-1.31	-1.26
3	-1.76	-1.40	-1.34
4	-1.86	-1.48	-1.42

DLS analysis

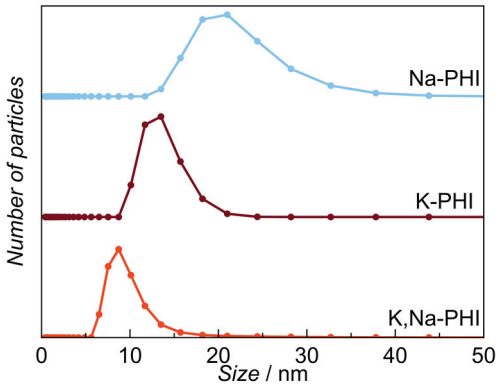

Figure S12. DLS particle size distribution of the poly(heptazine imide) samples.

SEM and TEM investigation

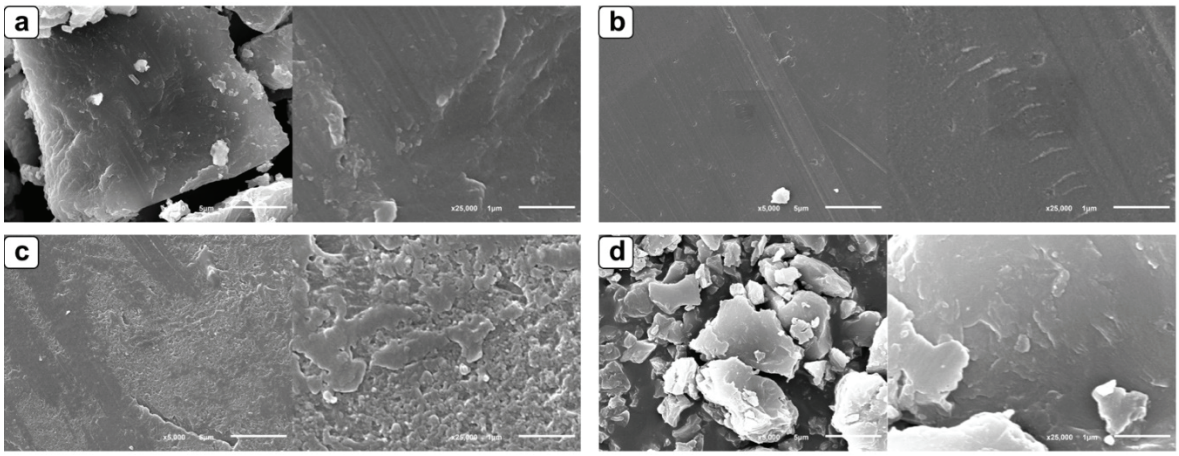

Figure S13. SEM images of the (a) K-PHI-S, (b) K-PHI, (c) Na-PHI and (d) K,Na-PHI samples.

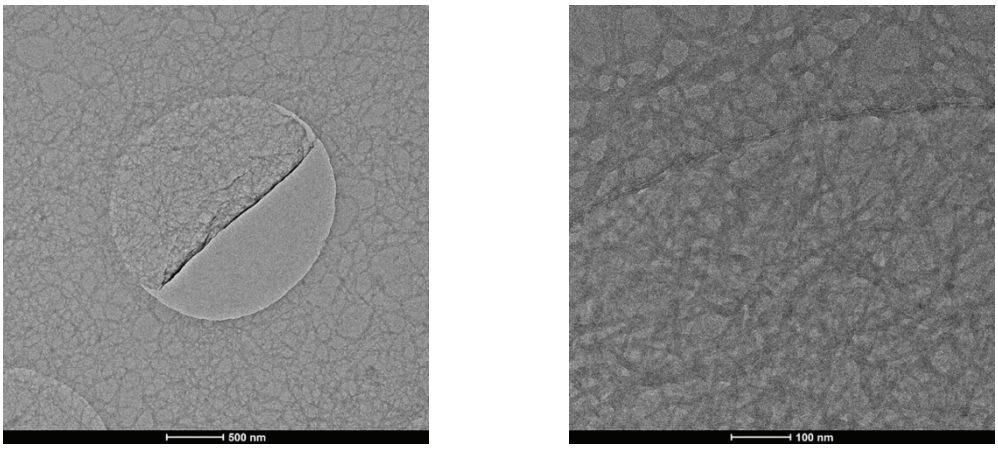

Figure S14. TEM images of the K,Na-PHI sample.

Photocatalytic studies

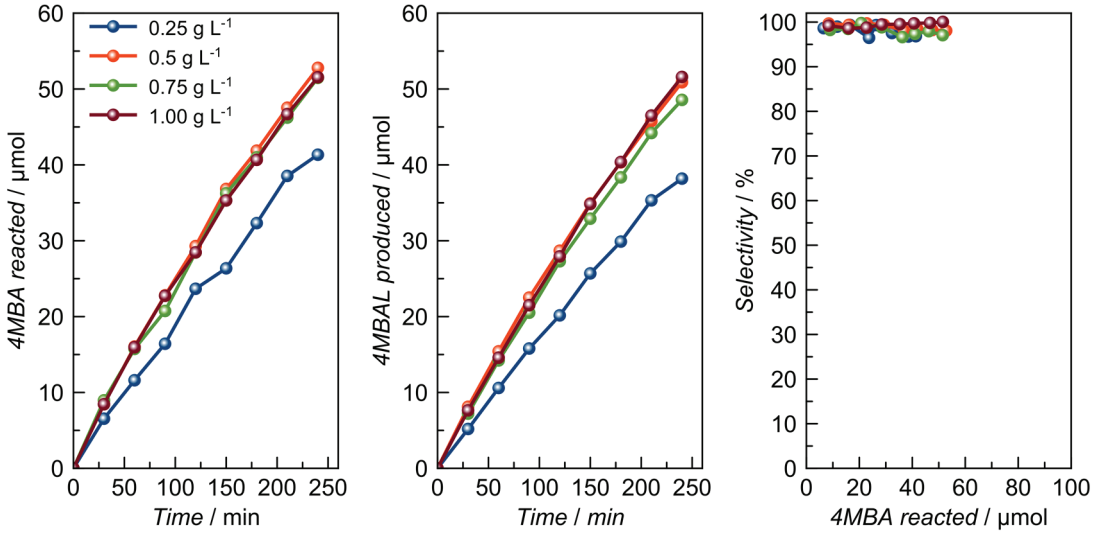

Figure S15. Photocatalytic 4MBA oxidation at different loadings of the K-PHI-S sample (20 mL, 4MBA 0.1 mmol, LED 365 nm).

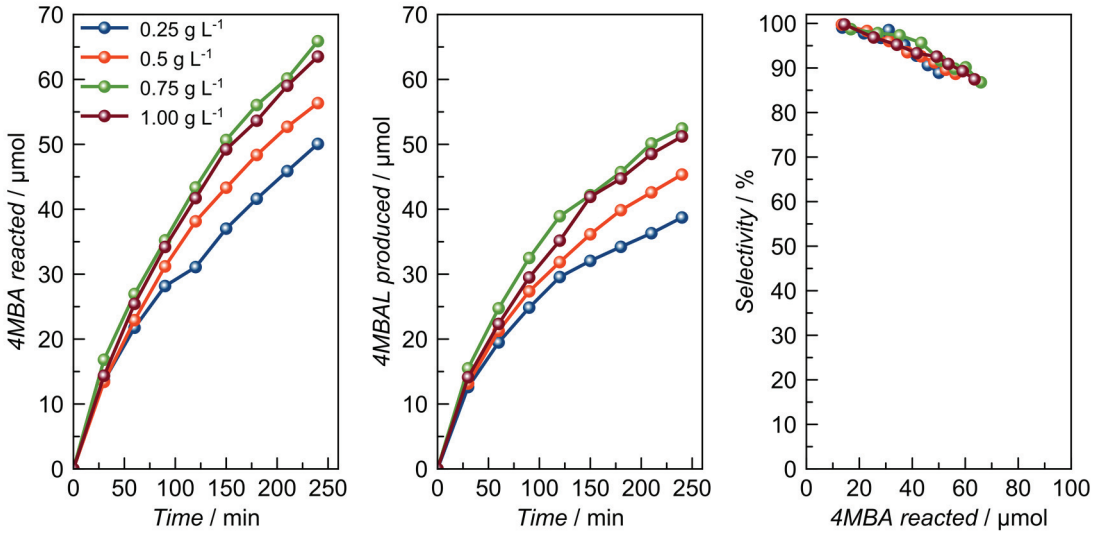

Figure S16. Photocatalytic 4MBA oxidation at different loadings of the K,Na-PHI sample (20 mL, 4MBA 0.1 mmol, LED 365 nm).

Table S6. Results of photocatalytic oxidation of 4MBA to 4MBAL with the concurrent H_2O_2 production

Sample	4MBA oxidation rate $*10^3$ / min^{-1}[a]	4MBA reacted in 4h / µmol	Selectivity to 4MBAL at 50% of 4MBA conversion / %	Selectivity to 4MBAL after 4 h / %	Selectivity to H_2O_2 after 4 h / %
CN H_2O	-1.4	28	-	≥ 99	97
K-PHI-S H_2O	-2.9	53	97	97	67
K,Na-PHI H_2O	-3.9	64	92	87	48
K,Na-PHI 10 % MeCN	-6.7	82	94	82	51
K,Na-PHI 20 % MeCN	-8.8	88	97	83	62
K,Na-PHI 40 % MeCN	-9.1	86	97	91	76
K,Na-PHI 50 % MeCN	-8.6	87	97	93	74
K,Na-PHI 70 % MeCN	-3.7	56	≥ 99	≥ 99	75
K,Na-PHI 85 % MeCN	-3.7	60	98	98	78

[a] The oxidation rate is quantified considering a pseudo-first order model with R^2 always ≥ 0.98

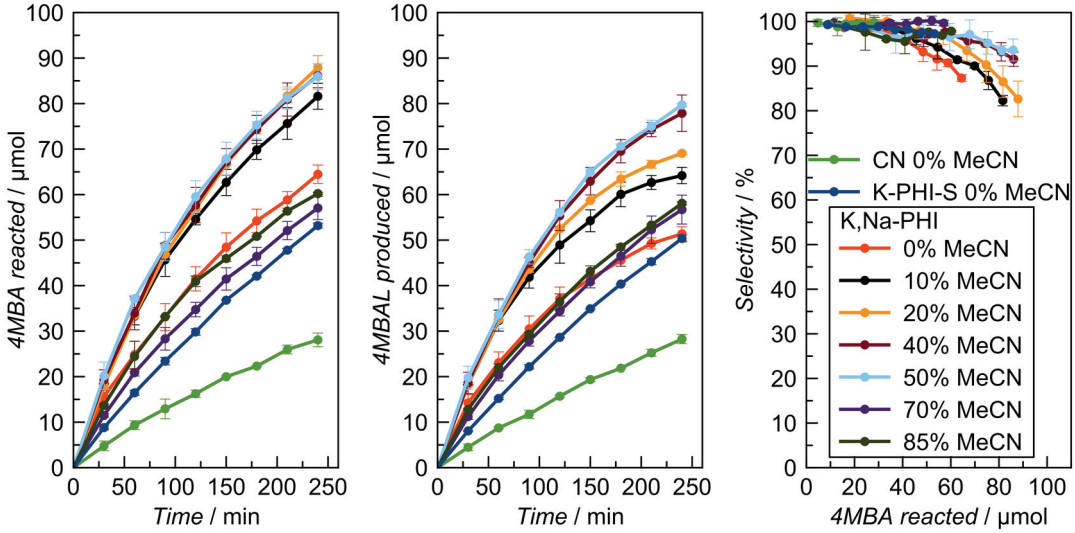

Figure S17. (a) Photocatalytic oxidation of 4MBA in H_2O (20 mL, 4MBA 0.1 mmol, LED 365 nm) and in H_2O/MeCN mixture in the presence of K,Na-PHI (20 mL, X vol% of MeCN, 4MBA 0.1 mmol, LED 365 nm).

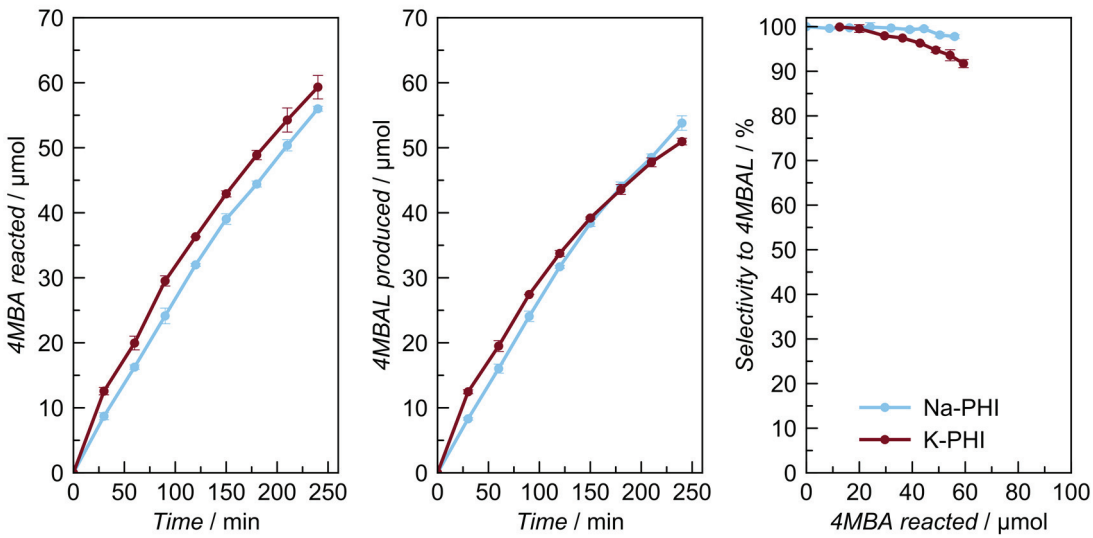

Figure S18. Photocatalytic 4MBA oxidation in the presence of the K-PHI and Na-PHI samples (20 mL, 4MBA 0.1 mmol, LED 365 nm).

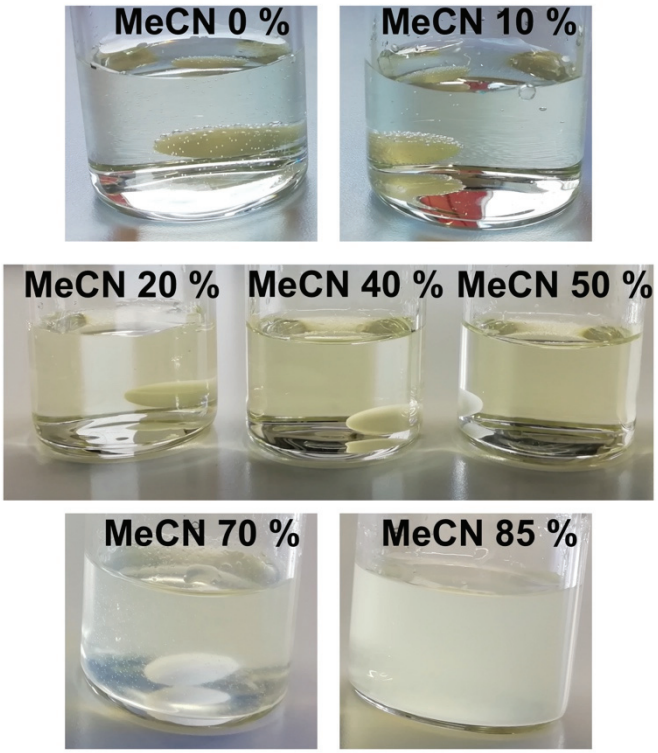

Figure S19. Photographs of the K,Na-PHI sample suspended in 4MBA solutions having varied MeCN vol. %.

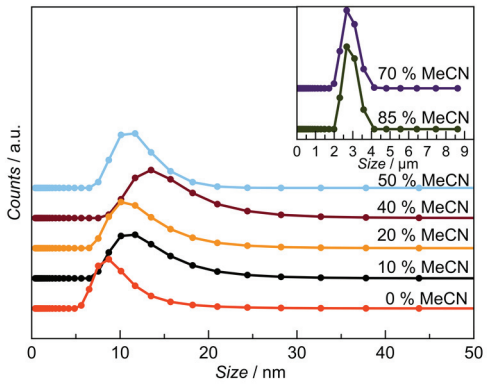

Figure S20. DLS particle size distribution of the K,Na-PHI sample suspended in 4MBA solutions having varied MeCN vol. %.

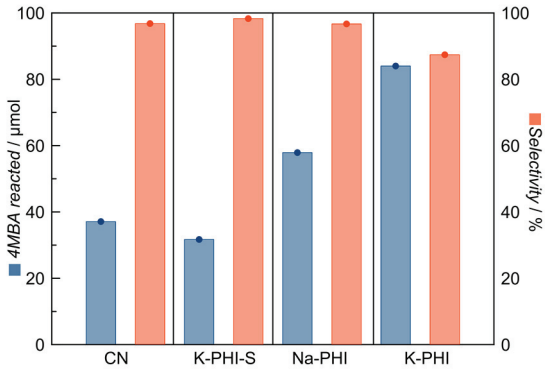

Figure S21. Conversion and selectivity of photocatalytic oxidation of 4MBA towards 4MBAL (0.1 mmol 4MBA, 20 mL, 40 vol.% MeCN, 365 nm) after 4 h of irradiation in presence of different photocatalysts.

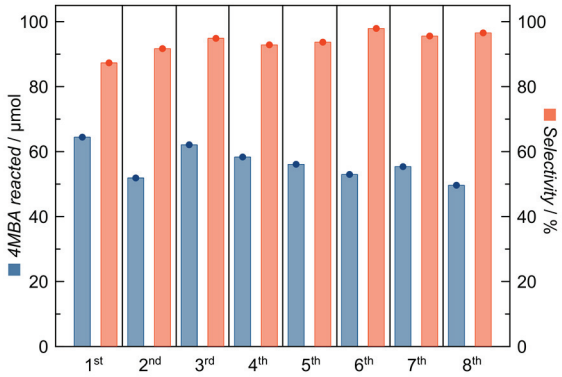

Figure S22. Recyclability test of the K,Na-PHI samples for 4MBA oxidation (20 mL, H_2O, 4MBA 0.1 mmol, LED 365 nm, 4 h of irradiation, 0.25 g of NaCl is added for the photocatalyst recovery)

References

1. G. Kresse, J. Hafner, *Phys. Rev. B* **1993**, *47*, 558–561.
2. G. Kresse, J. Hafner, *Phys. Rev. B* **1994**, *49*, 14251–14269.
3. G. Kresse, J Furthmüller, *Comput. Mater. Sci.* **1996**, *6*, 15–50.
4. G. Kresse, J. Furthmüller, *Phys. Rev. B* **1996**, *54*, 11169–11186.
5. G. Kresse, D. Joubert, *Phys. Rev. B* **1999**, *59*, 1758–1775.
6. J. P. Perdew, K. Burke, M. Ernzerhof, *Phys. Rev. Lett.* **1996**, *77*, 3865–3868.
7. D. Gunceler, K. Letchworth-Weaver, R. Sundararaman, K. A. Schwarz, T. A. Arias, *Model. Simul. Mater. Sci. Eng.* **2013**, *21*, 074005.
8. K. Mathew, R. G. Hennig, *ArXiv160103346 Cond-Mat* (2016).
9. K. Mathew, R. Sundararaman, K. Letchworth-Weaver, T. A. Arias, R. G. Hennig, *J. Chem. Phys.* **2014**, *140*, 084106.
10. H. J. Monkhorst, *Phys. Rev. B* **1976**, *13*, 5188–5192.
11. A. P. Dementjev,et al. *Diamond Relat. Mater.* **2000**, *9***,** 1904-1907
12. D. L. Zu, et al. *J. Mater. Sci*. **2007**, *43***,** 689-695